













## Schlafen 12 restricts HIV-1 latency reversal by a codon-usage dependent post-transcriptional block in CD4<sup>+</sup> T cells

Mie Kobayashi-Ishihara <sup>1,16,17,18</sup>✉, Katarína Frazão Smutná<sup>1,17</sup>, Florencia E. Alonso<sup>1</sup>, Jordi Argilagué<sup>1,2,3</sup>, Anna Esteve-Codina <sup>4</sup>, Kerstin Geiger<sup>1</sup>, Meritxell Genescà <sup>5</sup>, Judith Grau-Expósito<sup>5</sup>, Clara Duran-Castells<sup>6</sup>, Selina Rogenmoser<sup>1</sup>, René Böttcher<sup>7</sup>, Jennifer Jungfleisch<sup>7</sup>, Baldomero Oliva <sup>8</sup>, Javier P. Martínez<sup>1</sup>, Manqing Li <sup>9</sup>, Michael David <sup>9,10</sup>, Makoto Yamagishi <sup>11</sup>, Marta Ruiz-Riol<sup>6,12</sup>, Christian Brander <sup>6,13,14</sup>, Yasuko Tsunetsugu-Yokota <sup>15</sup>, Maria J. Buzon <sup>5</sup>, Juana Díez <sup>7,18</sup>✉ & Andreas Meyerhans <sup>1,14,18</sup>✉

Latency is a major barrier towards virus elimination in HIV-1-infected individuals. Yet, the mechanisms that contribute to the maintenance of HIV-1 latency are incompletely understood. Here we describe the Schlafen 12 protein (SLFN12) as an HIV-1 restriction factor that establishes a post-transcriptional block in HIV-1-infected cells and thereby inhibits HIV-1 replication and virus reactivation from latently infected cells. The inhibitory activity is dependent on the HIV-1 codon usage and on the SLFN12 RNase active sites. Within HIV-1-infected individuals, *SLFN12* expression in PBMCs correlated with HIV-1 plasma viral loads and proviral loads suggesting a link with the general activation of the immune system. Using an RNA FISH-Flow HIV-1 reactivation assay, we demonstrate that SLFN12 expression is enriched in infected cells positive for HIV-1 transcripts but negative for HIV-1 proteins. Thus, codon-usage dependent translation inhibition of HIV-1 proteins participates in HIV-1 latency and can restrict the amount of virus release after latency reversal.

<sup>1</sup>Infection Biology Group, Department of Medicine and Life Sciences, Universitat Pompeu Fabra, Barcelona, Spain. <sup>2</sup>Unitat mixta d'Investigació IRTA-UAB en Sanitat Animal. Centre de Recerca en Sanitat Animal (CRESA), Campus de la Universitat Autònoma de Barcelona (UAB), Bellaterra, Spain. <sup>3</sup>IRTA. Programa de Sanitat Animal. Centre de Recerca en Sanitat Animal (CRESA), Campus de la Universitat Autònoma de Barcelona (UAB), Bellaterra, Spain. <sup>4</sup>Centro Nacional de Análisis Genómico (CNAG-CRG), Center for Genomic Regulation (CRG), Barcelona Institute of Science and Technology, Barcelona, Spain. <sup>5</sup>Infectious Disease Department, Hospital Universitari Vall d'Hebrón, Institut de Recerca (VHIR), Universitat Autònoma de Barcelona, Barcelona, Spain. <sup>6</sup>IrsiCaixa AIDS Research Institute, Hospital Germans Trias i Pujol, Universitat Autònoma de Barcelona, Badalona, Spain. <sup>7</sup>Molecular Virology Group, Department of Medicine and Life Sciences, Universitat Pompeu Fabra, Barcelona, Spain. <sup>8</sup>Structural Bioinformatics Group, Department of Medicine and Life Sciences, Universitat Pompeu Fabra, Barcelona, Spain. <sup>9</sup>Section of Molecular Biology, Division of Biological Sciences, University of California San Diego, La Jolla, CA, USA. <sup>10</sup>Moore's Cancer Center, University of California San Diego, La Jolla, CA, USA. <sup>11</sup>Graduate School of Frontier Sciences, The University of Tokyo, Tokyo, Japan. <sup>12</sup>CIBER de Enfermedades Infecciosas, Madrid, Spain. <sup>13</sup>Universitat de Vic-Universitat Central de Catalunya (UVic-UCC), Vic, Spain. <sup>14</sup>Institució de Recerca i Estudis Avançats (ICREA), Barcelona, Spain. <sup>15</sup>Department of Medical Technology, School of Human Sciences, Tokyo University of Technology, Tokyo, Japan. <sup>16</sup>Present address: Department of Molecular Biology, Keio University School of Medicine, Tokyo, Japan. <sup>17</sup>These authors contributed equally: Mie Kobayashi-Ishihara, Katarína Frazão Smutná. <sup>18</sup>These authors jointly supervised this work: Mie Kobayashi-Ishihara, Juana Díez, Andreas Meyerhans. ✉email: [mieki@keio.jp](mailto:mieki@keio.jp); [juana.diez@upf.edu](mailto:juana.diez@upf.edu); [andreas.meyerhans@upf.edu](mailto:andreas.meyerhans@upf.edu)

The main obstacle in curing an established HIV-1 infection is the long-lived reservoir of latently infected CD4+ T cells<sup>1</sup>. These cells are treatment-resistant and therefore enable the persistence of HIV-1 proviruses despite combination antiretroviral therapy (cART) and antiviral immune responses. Once cART is interrupted, HIV-1 rapidly rebounds from the viral reservoir even after years-long treatment periods<sup>1</sup>. During treatment, the reservoir is maintained by T cell expansion that can be activated by (i) antigen-driven proliferation, (ii) integration-site-driven proliferation, and (iii) homeostatic proliferation (Reviewed in refs. 2,3). Consequently, targeting the mechanisms governing the expansion of infected T cells represents a potential treatment strategy in HIV-1 cure attempts.

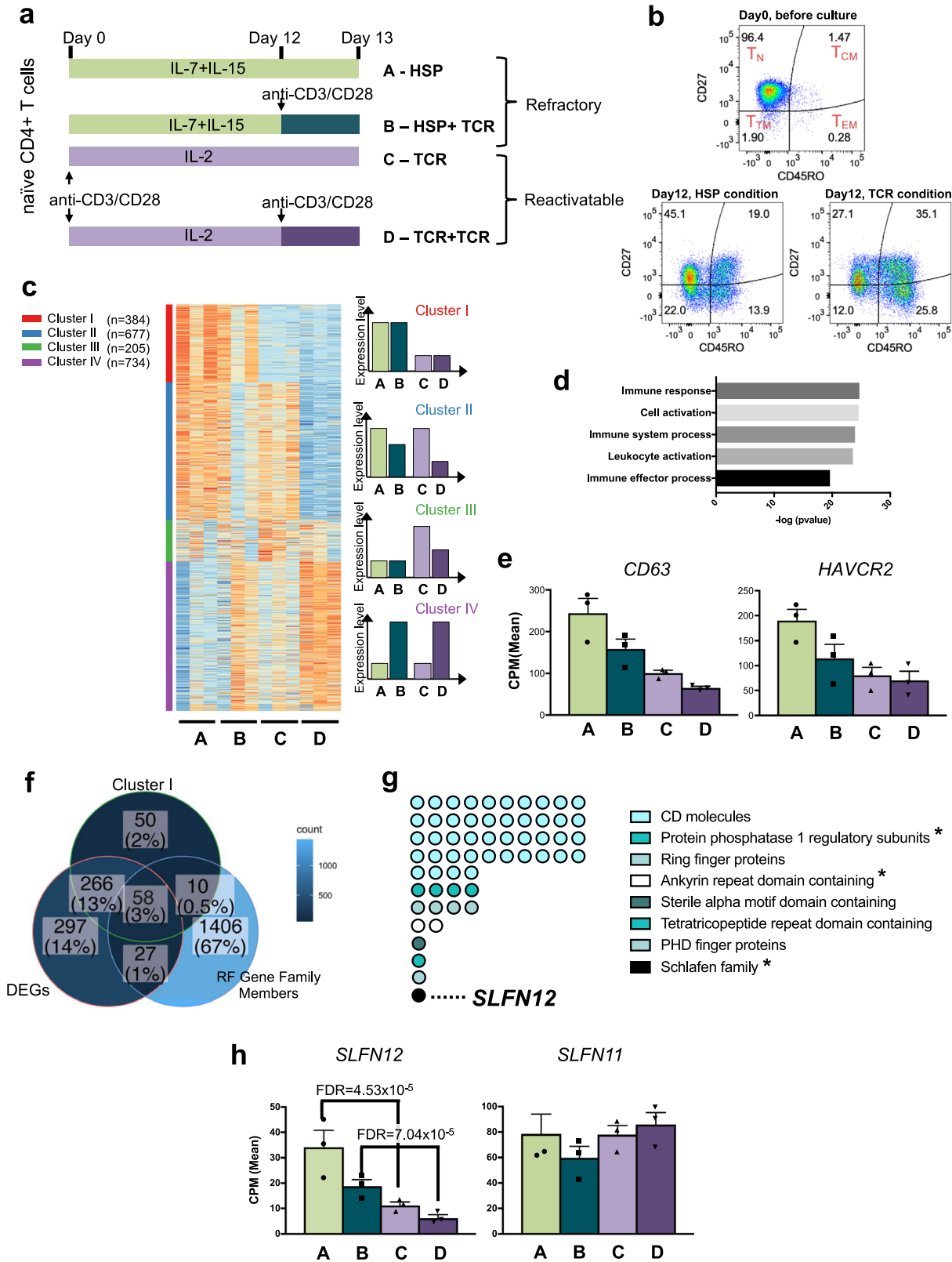
Antigen-driven proliferation triggered by T cell receptor (TCR) signaling is a strong physiological inducer of CD4+ T cell expansion. While this also reactivates latent HIV-1 and thus, can be the source of viral rebound<sup>4,5</sup>, sequential waves of polyclonal T cell stimulation in the presence of cART may result in viral reservoir reduction according to the “rinse and replace” strategy<sup>6</sup>. Latently infected T cells may also expand clonally when virus integration takes place within cancer-associated genes that affect cell proliferation<sup>7–10</sup>. Given the observed enrichment for such integration events over non-cancer-associated genes, this expansion mechanism seems common<sup>10</sup>. Nonetheless, latency reversal depends on position effects i.e., the exact location of the provirus within the chromosome<sup>11</sup> and thus, the mere expansion of infected T cell clones does not necessarily guarantee provirus transcriptional activity. Finally, infected CD4+ T cells may expand through homeostatic proliferation (HSP) driven by interleukins IL-7 and IL-15. Unlike antigen-driven proliferation, HSP allows the expansion of HIV-1-infected CD4+ T cells without activating HIV-1 expression<sup>12,13</sup>. While these conditions strongly activate STAT5 signaling<sup>14,15</sup>, the mechanisms for HIV-1 containment are unknown. Our previous work using HIV-1-infected primary CD4+ T cells maintained under HSP culture conditions suggested a post-transcriptional block as a cause of the containment<sup>16</sup>. Here we demonstrate that *SLFN12*, a member of a conserved family of proteins with antiviral activities, participates in the maintenance of HIV-1 latency and may enable to replenish the HIV-1 reservoir pool during homeostatic proliferation in vivo.

## Results

***SLFN12* is differentially expressed in homeostatic proliferating primary CD4+ T cells and is a candidate for post-transcriptional blockage of HIV-1.** To decipher the mechanisms that contribute to the HIV-1 refractory state in homeostatic proliferating CD4+ T cells, we analyzed differentially expressed genes in primary CD4+ T cells that were cultured either under HSP conditions or after TCR-stimulation. For this, naive CD4+ T cells were purified from peripheral blood mononuclear cells (PBMCs) of three HIV-1 uninfected blood donors (purity > 90%) and cultured in four different ways schematically shown in Fig. 1a, A–D; cultures with IL-7 and IL-15 (HSP-cultured CD4+ T cells) after stimulation via the TCR at day 12 (B; HSP + TCR) or not stimulated (A; HSP), and cultures with IL-2 after anti-CD3/CD28 activation (TCR-cultured CD4+ T cells) with a second TCR activation at day 12 (D; TCR + TCR) or without (C; TCR). Around half of the cells maintained their naive phenotype under HSP culture conditions whereas the majority of cells became memory cells under TCR conditions (Fig. 1b). On day 13, RNA was isolated from the cultured cells and transcriptomes analyzed by RNA-seq (Supplementary Data 1). Genes were ranked by their standard deviation across the four culture conditions. The top 2000 variably expressed genes were classified into

four main groups, referred to as clusters I to IV by k-means clustering<sup>17</sup> (Fig. 1c and Supplementary Data 2). Genes of cluster I ( $n = 384$ ) are upregulated in both HSP and HSP + TCR conditions compared to either TCR or TCR + TCR conditions. Since our previous work demonstrated that HIV-1 proviruses in HSP condition, but not TCR conditions, were refractory to TCR activation (HSP + TCR condition)<sup>16</sup>, cluster I is expected to contain candidate factors that contribute to HIV-1 restriction. GO analysis of the cluster I genes showed significant enrichment of the terms *immune response*, *cell activation* and *immune system process* (Fig. 1d). Ten of these genes were reported to be linked to HIV-1 inhibition according to the NIH HIV interactome database<sup>18–20</sup> (Supplementary Data 3). For example, *CD63* has been shown to repress HIV-1 infection<sup>21–24</sup> and *HAVCR2* inhibits viral budding<sup>25</sup> (Fig. 1e).

To further narrow down candidate restriction factors, we selected from the cluster I genes those that are (i) differentially expressed either in HSP vs TCR, or in HSP + TCR vs TCR + TCR (FDR < 5%, Supplementary Data 4), and that are (ii) members of a gene family that contains a known restriction factor (RF). The latter criterion was used because RF-containing gene families often have members with partially redundant functions to safeguard an organism against pathogenic threats<sup>26,27</sup>. A family member list was therefore created that includes known restriction factors<sup>28</sup>. It is given in Supplementary Data 4. From the total of 1,501 family members, 58 genes fulfill the above criteria as candidate RFs for HIV-1 latency control (Fig. 1f). Among these 58 candidates, 44 gene products were attributed to clusters of differentiation (CD) molecules like the restriction factor *CD317* (*BST2* = *Tetherin*) (Fig. 1g and Supplementary Data 5). However, since our previous work pointed to a post-transcriptional restriction of HIV-1 in HSP condition cultured CD4+ T cells<sup>16</sup>, we paid particular attention to members of three gene families that could potentially be involved in post-transcriptional and/or translational events (Fig. 1g). Protein phosphatase 1 regulatory subunits (PPP1Rs) are a gene family whose members interact with and regulate serine/threonine phosphatases. One of these is *EIF2AK2* (also known as Protein kinase R) that senses viral RNAs and enhances the integrated stress response (ISR)<sup>29–31</sup>, which enables the shutdown of global protein synthesis<sup>32</sup>. Four other family members are *PPP1R9A*, *BCL2L2*, *AATK*, and *SPRED1* (Supplementary Fig. 1). *PPP1R9A* is predicted to interact with F-actin and inhibits protein phosphatase 1- $\alpha$  activity<sup>33</sup>. *BCL2L2* encodes a BCL2-like protein which is usually involved in apoptosis and thus could contribute to cell expansion under HSP conditions<sup>34</sup>. *AATK* is a serine/threonine-protein kinase, which is likely involved in neuronal differentiation<sup>35</sup>. *SPRED1* activates MAP-kinase signaling<sup>36</sup>. Although these proteins have various functions, they all have the potential to deactivate translation factors by modifying their phosphorylation status in response to a viral infection. In addition, the candidate genes *UACA* and *ANKRD50* are members of the Ankyrin repeat family to which *RNASEL* (RNase L) also belongs (Supplementary Fig. 1). RNase L can cleave viral RNAs to induce inflammatory responses<sup>37,38</sup>. The Ankyrin domain of RNase L is critical to forming functional dimers and sensing viral RNAs<sup>39</sup>. While the function of *ANKRD50* has not been well characterized, *UACA* is a known repressor of NF- $\kappa$ B transcription<sup>40,41</sup> and these proteins may together participate in viral RNA sensing and innate immune activation within HSP-cultured CD4+ T cells. Finally, within cluster I there was *SLFN12*, a member of the Schlafen protein family (*SLFN*). This protein has been identified in two high-throughput screenings for interferon-induced antiviral and anti-retroviral factors<sup>42,43</sup>. It has moderate activity against vesicular stomatitis virus (VSV)<sup>43</sup> and a mouse gammaherpes virus (MHV-68)<sup>43</sup> as well as activity against several retroviruses including HIV-1<sup>42</sup>. Its mechanism of antiviral activity has not yet been



studied. For several of the other SLFN proteins, effective antiviral functions have been reported (recently reviewed by Kim et al.<sup>44</sup>). SLFN11 was shown to be a restriction factor (RF) repressing HIV-1 protein translation<sup>45</sup>. Other human SLFN proteins namely SLFN5, SLFN13 and SLFN14 are known to attenuate the production of several viruses including influenza virus, retroviruses, and flaviviruses<sup>46–49</sup>. Based on these descriptions of SLFN genes and

the statistical signal observed in our in vitro stimulation, we hypothesized that SLFN12 might be another member of the SLFN family with an anti-HIV-1 activity that might act at a post-transcriptional level.

To first confirm SLFN12 gene expression in CD4+ T cells under HSP and TCR culture conditions, CD4+ T cells from five additional healthy blood donors were cultured under the respective

**Fig. 1 Differential RNA-seq analysis of cultured naive CD4+ T cells to identify candidate HIV-1 restriction factors.** **a** Scheme of naive CD4+ T cell cultures. Naïve CD4+ T cells from 3 different HIV-1-negative blood donors were maintained for 13 days under 4 different conditions: IL-7+IL-15 alone (A-HSP) or with anti-CD3/CD28 activation at day 12 (B-HSP+ TCR); IL-2 after anti-CD3/CD28 activation alone (C-TCR) or with a second activation by anti-CD3/CD28 at day 12 (D-TCR+ TCR). On day 13, total RNA was isolated and processed for transcriptome analysis to identify candidate HIV-1 restriction factors. **b** Phenotypes of CD4+ T cells maintained under HSP or TCR condition. A representative result of one of the three blood donors utilized in **a** is shown. Isolated naive CD4+ T cell purity was above 91%, and 96.5% for the donor shown in the upper panel. After 12-day cultivation, a naïve T cell phenotype is partially maintained in HSP conditions (CD27+/CD45RO-, 45.1%; on average >30%), while TCR conditions increased cells with central memory phenotype (CD27+/CD45RO+, 35.1%; on average >35%). T<sub>N</sub>, naïve T cells; T<sub>CM</sub>, central memory T cells; T<sub>EM</sub>, effector memory T cells; T<sub>TM</sub>, terminally differentiated memory T cells. **c** Heatmap of the top 2,000 variable genes clustered by k-means analysis (red: upregulated, blue: downregulated). Four main clusters were identified: Cluster I, genes upregulated in both HSP and HSP + TCR conditions compared to either TCR or TCR + TCR conditions ( $n = 384$ ). Cluster II, genes upregulated in HSP, HSP + TCR and TCR conditions ( $n = 677$ ). Cluster III, genes with a trend to be upregulated in TCR condition ( $n = 205$ ). Cluster IV, genes upregulated by TCR stimulation at day12 ( $n = 734$ ). These differences in expression are visualized on the right panel for clarity. **d** Top 5 gene ontology terms of the cluster I genes. **e** Expression patterns of two known inhibitors of HIV-1 replication/function in the cluster I according to the NIH HIV interaction database<sup>18–20</sup>. Mean counts per million reads (CPM) and the standard error of the mean (SEM;  $n = 3$ ) are shown. **f** Venn diagram shows overlap among (i) cluster I genes, (ii) differentially expressed genes in HSP vs TCR and in HSP + TCR vs TCR + TCR conditions (DEGs), and (iii) members of gene families that contain a known restriction factor (RF gene family members). **g** Candidate restriction factors identified in **f** and their corresponding gene families. The asterisks show gene families that could potentially be involved in post-transcriptional and/or translational events. **h** Expression pattern of *SLFN11* and *SLFN12* from 3 blood donors. Plots represent mean CPM  $\pm$  SEM.

conditions (Fig. 1a) and *SLFN12* mRNAs were quantified by qPCR (Supplementary Fig. 2). The expression pattern was consistent with that of the RNA-seq analysis (Fig. 1h) and differed from the other SLFN family mRNAs that we analyzed in comparison (Supplementary Figs. 2 and 3). Indeed, these other SLFNs did not show a trend towards a decrease from HSP + TCR to TCR culture conditions and thus were considered non-consistent with a cluster I expression pattern (Fig. 1c).

**SLFN12 inhibits HIV-1 reactivation in a post-transcriptional process.** To establish a suitable in vitro model of viral reactivation and SLFN12 modulation, we evaluated different cell lines for *SLFN* gene expression profiles (T cell lines Jurkat, A3.01, ACH2 and embryonic kidney cells HEK 293T; Fig. 2a). *SLFN5* was expressed in all cell lines and was the only *SLFN* family member expressed in HEK 293T cells. *SLFN14* expression was not found in any of the tested cells. *SLFN11* and *SLFN12* were expressed in Jurkat, A3.01 cells and in HIV-1 latently infected ACH2 cells. Importantly, ACH2 cells had a similar expression pattern of *SLFN11* and *SLFN12* as primary CD4+ T cells under HSP culture conditions. Therefore, given that HSP has been suggested to maintain the HIV-1 latent reservoir and that the ACH2 cell line is an established model for HIV-1 latency, we used ACH2 cells to study the effect of *SLFN12* on HIV-1 reactivation. *SLFN11* has been shown to restrict HIV-1 at a translational level<sup>45</sup> and was used as a positive control for the subsequent experiments.

To knockdown *SLFN12* expression in ACH2 cells, we first generated retroviral vectors expressing specific shRNAs against *SLFN12* (shSLFN12#1/ shSLFN12#2), *SLFN11* (shSLFN11) or expressing a scrambled shRNA (shSc) as control. ACH2 cells were then transduced with these vectors and HIV-1 was reactivated by treatment with the HDAC inhibitor SAHA (also known as Vorinostat) as shown schematically in Fig. 2b. Cell lysates and supernatants (SN) were harvested at 48 and 72 h (h) post-reactivation, respectively, and analyzed. The mRNAs of *SLFN12* or *SLFN11* were roughly 60% suppressed by the specific shRNAs (Fig. 2c). After treatment with SAHA or the vehicle control DMSO, virus-containing supernatants from ACH2 cells were titrated using TZM-bl cells. Knockdown of *SLFN12* (*SLFN11*) expression resulted in at least 5.7-fold (2.8-fold) increase in infectious HIV-1 production (Fig. 2d). Moreover, the translation efficiency of HIV-1 Gag-Pr55 significantly increased (Fig. 2e,  $p < 0.05$ ), indicating that *SLFN12*, as *SLFN11*, control HIV-1 reactivation from latently infected T cells by repressing the translation efficiency of Gag-Pr55.

**SLFN12 restricts HIV-1 production by selectively inhibiting virus protein translation.** HEK 293T cells do not express *SLFN11* or *SLFN12* (Fig. 2a). To test how *SLFN12* influences HIV-1 replication, we co-transfected HEK 293T cells with pmCherry-SLFN11 (positive control), pmCherry-SLFN12 or empty pmCherry vector (mock) together with the HIV-1 pNL-E vector, an HIV-1 provirus clone encoding *EGFP* between the *env* and *nef* coding region<sup>50</sup> (Fig. 3a). Expression system of SLFN proteins was confirmed by Western blots (Fig. 3b). 48 h post-transfection, supernatants and cell lysates were collected for further analyses. *SLFN12* affected HIV-1 production and strongly diminished HIV-1 titres as well as Gag-p24 protein in supernatants in a dose-dependent manner (Fig. 3c, d). This decrease was unlikely due to inhibitory effects on viral RNA processing or export (Fig. 3e, f, Supplementary Fig. 4). Western blot analysis with specific antibodies showed down-regulation of Gag-p24 and the Nef accessory protein (Fig. 3g). However, we did not observe any change in cellular GAPDH or enhanced green fluorescent protein (EGFP) derived from the pNL-E vector. Thus, *SLFN12*, as *SLFN11*, inhibit HIV-1 production by selectively reducing translation of at least some viral proteins.

**SLFN12 affects the translational machinery to stall ribosomes on HIV-1 mRNA.** To determine how *SLFN12* may influence the process of translation of viral proteins, we co-transfected HEK 293T cells with *SLFN* vectors and pNL-E, and performed a polysome profiling analysis (Fig. 4a). UV absorbance profiles showed no significant differences in total cellular RNA distribution among the three transfected cells (Fig. 4b). Given similar monosome to polysome ratios (Fig. 4c), *SLFN12*, as well as *SLFN11*, seems not to affect global mRNA translation. Next, we analyzed the distribution of *GAPDH* mRNAs, whose expression levels are not affected by *SLFN12* or *SLFN11* expression (Fig. 3g), and HIV-1-*gag* mRNAs within monosome and polysome fractions. *GAPDH* mRNAs were mainly distributed in light polysomes even in the presence of the SLFN proteins (Fig. 4d, fractions 8–12, 13–17, and 18–23). However, upon *SLFN12* or *SLFN11* expression, HIV-1-*gag* mRNAs were shifted from light polysomes towards heavy, elongating polysomes (Fig. 4e). This increase of ribosomes per HIV-1 *gag* mRNA, together with the observed inhibition of HIV-1-p24 expression levels (Fig. 3g), is concordant with slow or stuck ribosomes i.e., slowing down translation elongation.

**Translational block by SLFN12 is codon-usage-dependent.** The translation elongation rate is severely affected by codon optimality



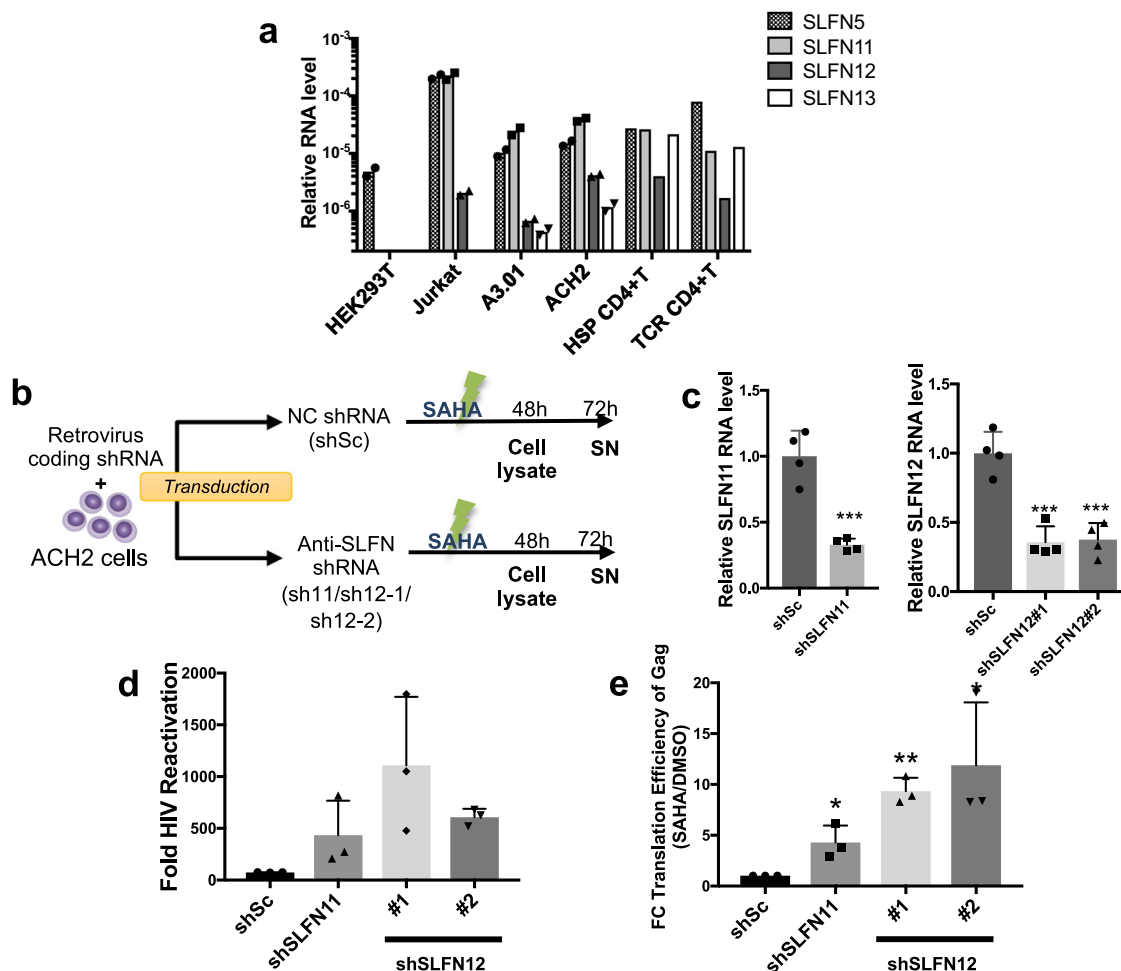


**Fig. 2** *SLFN12* affects HIV-1 latency reversal from ACH2 cells. **a** Relative transcript levels of the human SLFN family members 5, 11, 12 and 13 in different cell lines (mean values of two repeated measurements) as well as in naive CD4+ T cells under HSP or TCR culture conditions. Naive CD4+ T cells were isolated from five independent HIV-1-negative blood donors and cultivated for 13 days with IL-7 + IL-15 (HSP condition) or with anti-CD3/CD28 antibodies + IL-2 (TCR condition) as in Fig. 1a. Transcripts were quantified by RT-qPCR with specific primer pairs and normalized to cellular *18S rRNA*. Dot plots of the individual values and p-values were provided in Supplementary Fig. 2. **b** Flow chart of *SLFNs* knockdown and HIV-1 reactivation. HIV-1 latently infected ACH2 cells were transduced with retroviral vectors expressing specific shRNAs against *SLFN11* (shSLFN11) or *SLFN12* (shSLFN12#1/shSLFN12#2), or with a scrambled shRNA (shSc) as a negative control. The cells were then treated with SAHA to reactivate HIV-1. DMSO at a concentration that equals the activation mix served as the vehicle control. Cell lysates and supernatants (SN) were harvested at 48- and 72-h post-reactivation, respectively, and analyzed. **c** Relative RNA levels of *SLFN11* (left panel) and *SLFN12* (right panel) in the knockdown ACH2 cells ( $n = 4$  biological replicates; mean  $\pm$  SD). \*\*\* represents  $p < 0.01$  by Student's *t* test. **d** SAHA-induced HIV-1 reactivation from ACH2 cells after *SLFN* knockdown. Fold HIV-1 reactivation was determined by titration of HIV-1-containing supernatants on TZM-bl cells and normalized to the basal HIV-1 level in DMSO-treated samples. Given is the mean  $\pm$  SD for three independent samples. **e** Knockdown of *SLFN11* and *SLFN12* in ACH2 cells increases translation efficiency of HIV-1 Gag-Pr55. Plots represent fold change (FC) translation efficiency of Gag-Pr55 in SAHA-treated samples to DMSO-treated samples. Pr55 translation efficiency was calculated as a ratio of cellular Pr55 protein levels to *gag* RNA levels. The cellular Pr55 protein and HIV-1 *gag* RNA levels were quantified by Western blot and RT-qPCR, respectively. The mean FC efficiency of the control knockdown cells (shSc) was set to 1. Results show the mean  $\pm$  SD of three independent experiments. Ratio paired *t*-test was used to calculate static significance (\* $p < 0.05$ , \*\* $p < 0.005$ ).

of transcripts and the availability of cognate transfer RNAs (tRNAs)<sup>51,52</sup>. *SLFN11* has been shown to inhibit HIV-1 translation in a codon-usage-dependent manner<sup>45</sup>. To test whether also *SLFN12* affects HIV-1 translation elongation in a codon-usage-dependent manner, we first compared viral codon frequencies to RefSeq-based human coding sequences using the Codon Adaptation Index (CAI), a general metric to analyze codon usage bias<sup>53</sup>. As previously described<sup>54</sup>, HIV-1 sequences harbor less optimal codons (lower CAI values) compared to most human transcripts including *GAPDH* (Fig. 5a). Next, we compared the effect of *SLFN12* on Gag-p24 protein production from wild-type (wt) and codon-optimized HIV-1-*gag* transcripts. For this, HEK 293T cells were co-transfected with the *SLFN12* expression vector plus a

vector expressing either HIV-1-*gag wt* (pGag-wt) or a codon-optimized HIV-1-*gag* (pGag-opt). Protein and mRNA levels were then analyzed 48 h later (Fig. 5b). Compared to mock, *SLFN12* strongly diminished translation of Gag-p24 protein transcribed from HIV-1-*gag wt* (Fig. 5c), however, protein expression in cells transfected with pGag-opt remained unchanged (Fig. 5d). Since the RNA levels of HIV-1-*gag wt* and HIV-1-*gag opt* were not significantly altered by *SLFN12*, HIV-1 inhibition by *SLFN12* (Fig. 3) may indeed occur at a post-transcriptional step.

To identify which codons may de-optimize the HIV-1 codon usage, we compared the relative synonymous codon usage (RSCU)<sup>55</sup> amongst HIV-1, HIV-2, Chikungunya virus (CHIKV) as an example of an unrelated virus, and humans (*H.sapiens*).

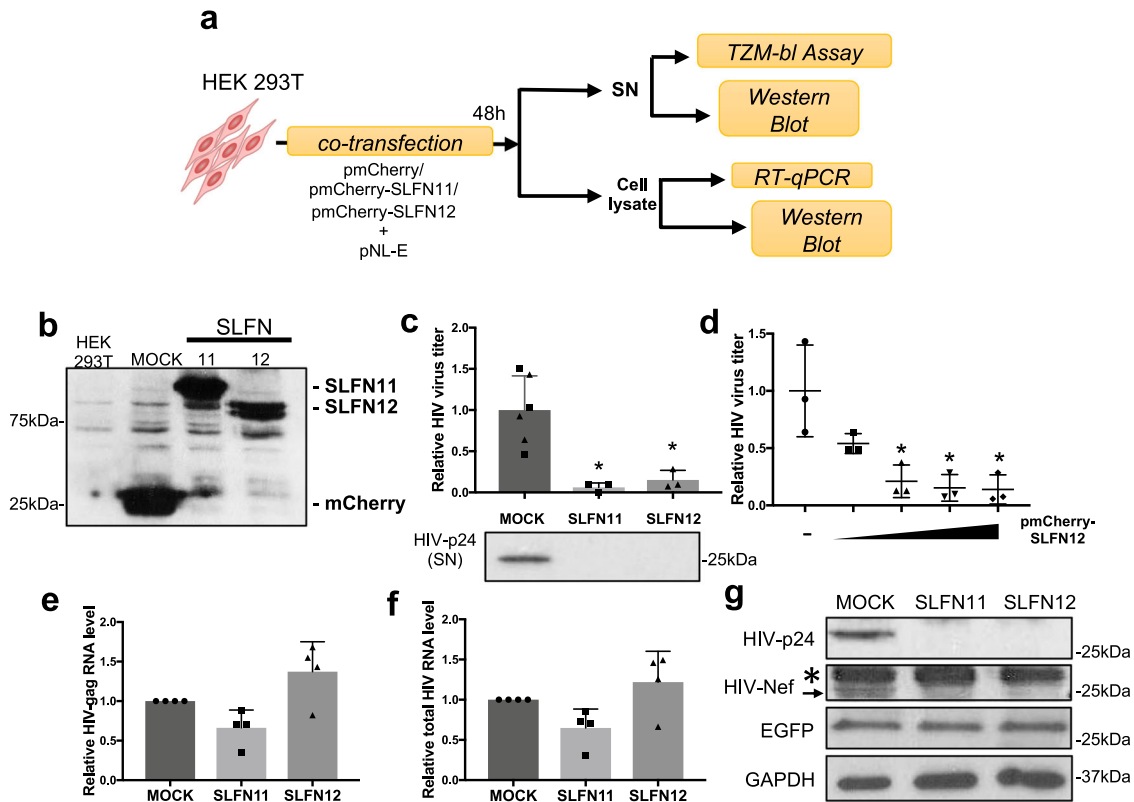


**Fig. 3** SLFN12 inhibits HIV-1 at the level of translation. **a** Experimental outline. HEK 293T cells were co-transfected with an expression plasmid encoding mCherry-fused SLFN11 or SLFN12, or mCherry alone, and the HIV-1 vector pNL-E. At 48 h post-transfection, supernatants (SN) and cell lysates were collected and processed for further analyses as indicated. **b** Expression of recombinant SLFN proteins in the transfected HEK 293T cells was studied by Western blots with an anti-mCherry antibody. **c** SLFN12 expression strongly diminishes HIV-1 production from transfected HEK 293T cells. Supernatants from the co-transfected cells were titrated by the TZM-bl assay (upper panel;  $n = 3$  for each SLFN11 (denoted as rectangles) or SLFN12 (triangles) independent transfection; mean  $\pm$  SD; \* $p < 0.05$  by Student's  $t$  test) and analyzed by Western blot (lower panel; a representative example of three independent experiments is shown). **d** Dose-dependent inhibition of HIV-1 production by SLFN12. HEK 293T cells were co-transfected with pNL-E and increasing amounts of pmCherry-SLFN12 (0, 0.2, 0.4, 0.8 or 1.6  $\mu$ g). The empty mCherry plasmid was added to maintain constant DNA amounts for all transfections. SNs were harvested 48 h after transfection and titrated by TZM-bl assay ( $n = 3$  biological replicates; mean  $\pm$  SD; \* $p < 0.05$  by Student's  $t$  test). SLFN12 expression did not significantly affect the levels of HIV-1 *gag* RNA (**e**) or total HIV-1 RNA (**f**). RNA levels were quantified by RT-qPCR and normalized to *18S rRNA* levels ( $n = 4$  biological replicates; mean  $\pm$  SD). There were no significant differences amongst the indicated samples (Student's  $t$  test). **g** Western blot from cell lysates of co-transfected HEK 293T cells with indicated antibodies. An arrow and asterisk highlight the bands of Nef and a nonspecific protein, respectively. Representative results of three independent experiments are shown.

As previously reported<sup>56,57</sup>, HIV-1 and -2 utilize many A-ending codons that are rare in humans and CHIKV (Fig. 5e and Supplementary Data 6). Among A-ending codons, both HIV-1 and HIV-2 use Leu-UUA very frequently instead of Leu-CUG that is common in humans. To test whether Leu codon swapping within *EGFP* would render its expression sensitive to SLFN12 inhibition, HEK 293T cells were co-transfected with the SLFN12 expression vector plus synonymous *EGFP* constructs differing in their codon usage. *EGFP* expression was analyzed by flow cytometry 48 h later (Fig. 5f). SLFN12 inhibited only Leu-UUA swapped *EGFP*. Altogether our results demonstrate that the attenuation of HIV-1 protein production by SLFN12 is codon-usage dependent.

**SLFN12-mediated HIV-1 suppression depends on a putative tRNase cleavage domain.** To better understand the mechanism by which SLFN12 may interfere with HIV-1 protein translation, we concentrated on the structural features of SLFN protein family members. The structure of SLFN12 was recently resolved by cryo-EM and suggested an RNase activity<sup>58,59</sup>. This was subsequently confirmed biochemically demonstrating a selective cleavage activity of SLFN12 for Leu-UUA tRNA<sup>60</sup>. SLFN11 and SLFN13 are also

known to degrade tRNAs<sup>49,61–63</sup>. Comparison of sequences and conformations of SLFN11, 12 and 13 showed a 34.8% similarity between SLFN12 and SLFN11 or SLFN13, and a 75.8% similarity between SLFN11 and SLFN13. Protein backbone structures were similar between the 3 proteins except that SLFN12 had a short C-terminal domain (Fig. 6a). Based on these structural and functional features, we hypothesized that SLFN12 may inhibit HIV-1 protein translation by cleaving the rare Leu-UUA tRNA and reduce its cellular concentration.

Leucine tRNAs are categorized as type II tRNAs that have an expanded variable loop compared to type I tRNAs<sup>64</sup>. We, therefore, simulated docking between the SLFN12 dimer and human type II tRNA structure available in the Uniplot database (Fig. 6b). A type II tRNA potentially fits into a space formed by the SLFN12 dimer. Furthermore, putative catalytic sites, which are composed of the negatively charged glutamic acids E200 and E205 in SLFN12, mapped closely to the docked tRNA. These putative RNase active sites were conserved as E209 and E214 in SLFN11<sup>63</sup>. Thus, SLFN12 may exert its codon-specific HIV-1 inhibitory effect through the two putative cleavage sites E200 and E205. To investigate this hypothesis, we generated expression vectors of SLFN11 and 12 in which the respective active site glutamic acids were converted

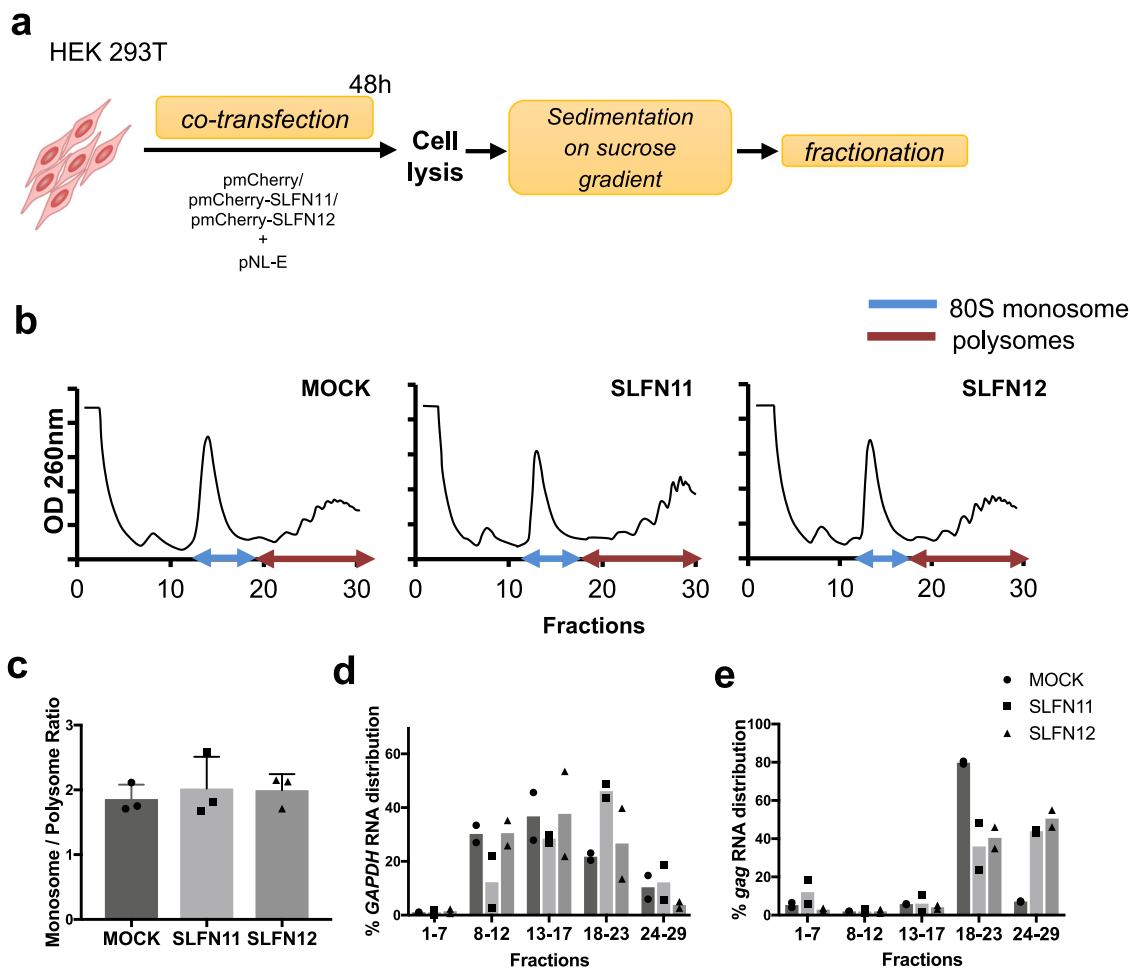
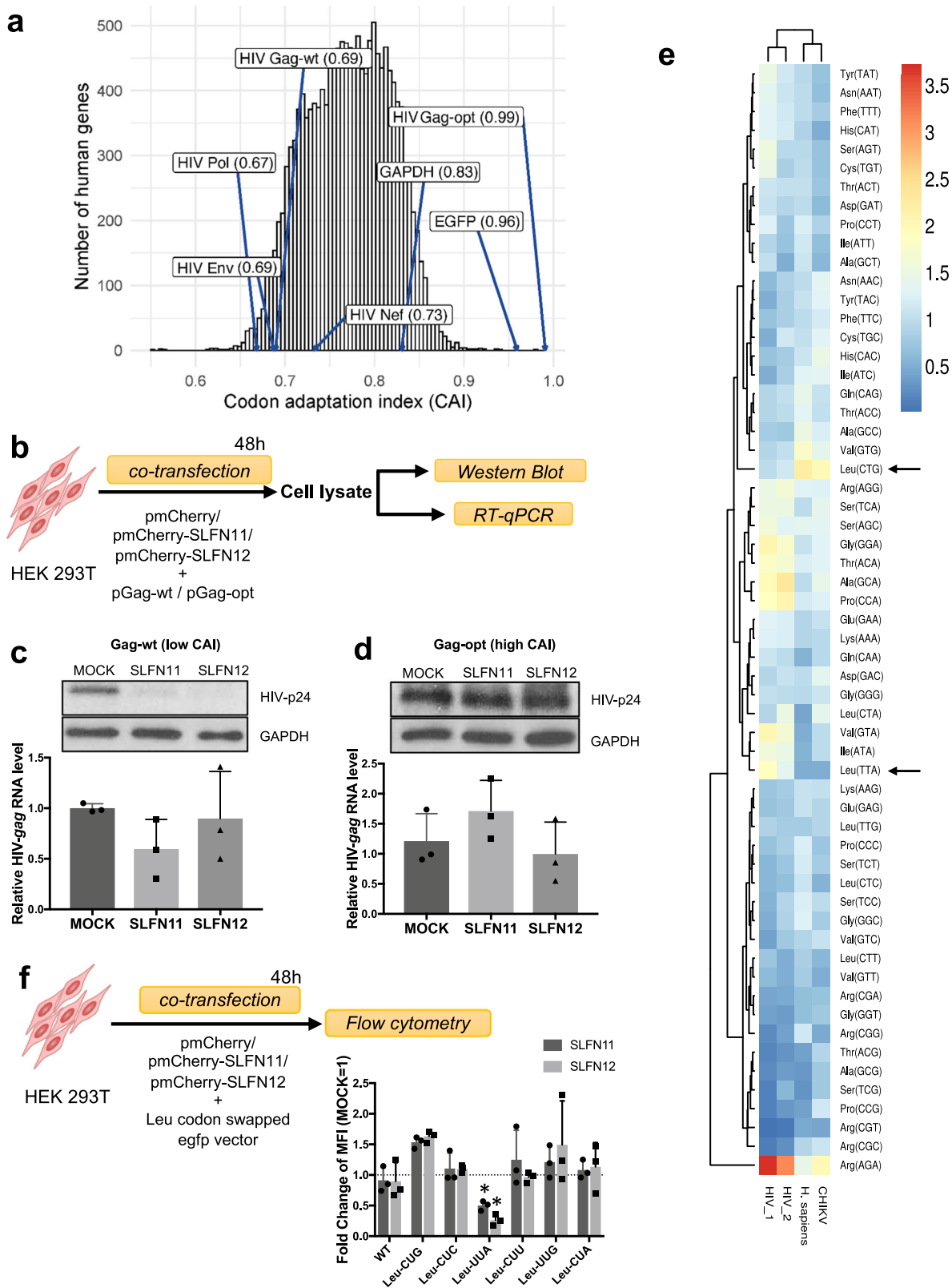


**Fig. 4 SLFN12 slows down translation elongation.** **a** Outline of polysome profiling. HEK 293T cells were co-transfected with expression plasmids encoding mCherry-fused SLFN11 or SLFN12, or mCherry alone, and the HIV-1 vector pNL-E. At 48 h post-transfection, cells were lysed and subjected to a 10–50% sucrose gradient centrifugation. The gradient was fractionated, and samples were processed for specific RT-qPCR shown in **d** and **e**. **b** UV absorbance profiles of lysed transfected HEK 293T cells after sucrose gradient fractionation (representative result of three independent samples). **c** SLFN12 expression does not influence the global ratio between monosomes and polysomes (mean  $\pm$  SD;  $n = 3$  biological replicates). **d, e** SLFN12 expression shifts the HIV-1 RNA distribution towards heavy polysomes. Distribution of GAPDH RNA (**d**) or HIV-1 gag RNA (**e**) in different fractions of HEK 293T cells expressing SLFN11 or SLFN12. Pooled fractions represent free proteins (mRNPs fraction; 1–7), single ribosomal subunits (40S + 60S; 8–12), 80S monosome (13–17), light- (18–23) and heavy -polysomes (24–29). The total amount of the RNAs in all fractions was set to 100% (mean  $\pm$  SD;  $n = 2$  biological replicates).

to alanine. HEK 293T cells were then co-transfected with the individual *SLFN* constructs and pNL-E, and the antiviral activity was tested by TZM-bl assays and Western blot (Fig. 6c). All active-site mutants of SLFN11 and SLFN12 reduced SLFNs anti-HIV-1 activity (Fig. 6d) and increased levels of Gag-Pr55 and its proteolyzed product, p24 (Fig. 6e). Likewise, these mutants lost their codon-dependent inhibition of Leu-UUA swapped-EGFP expression as shown by the increase of mean fluorescence intensities of HEK 293T cells co-transfected with Leu-UUA swapped-EGFP plus the individual *SLFN* mutants (Fig. 6f). Together these results demonstrate that the putative tRNA cleavage active sites E200 and E205 of SLFN12 mediate the post-transcriptional, codon-dependent blockage of HIV-1.

To test whether SLFN12 degrades tRNAs, we quantified tRNAs in SLFN-transfected cells by RNA gel electrophoresis. Visual inspection of the ethidium bromide-stained polyacrylamide gel showed a slight decrease in type II tRNA abundance (Supplementary Fig. 5a). Likewise, type I and II tRNA quantification by image J normalized to 5.8S or 5S rRNA levels showed a decrease in type II tRNA by SLFN12, although with less activity than the positive control SLFN11 (Supplementary Fig. 5b, c).

**Involvement of SLFN12 in HIV-1 post-transcriptional restriction within infected individuals.** To study SLFN12 expression and its putative role in the control of HIV-1 latency in HIV-1-infected individuals, we first analyzed *SLFN12* expression in PBMCs from HIV-1 high (High,  $n = 16$ ) and low viremic (Low,  $n = 30$ ) individuals, viremic controllers (VC,  $n = 11$ ), and elite controllers (EC,  $n = 12$ ). *SLFN12* mRNA expression levels per CD4 count showed significant differences among each group, and a tendency to increase with disease progression (Fig. 7a). The *SLFN12* mRNA level was also positively correlated with viral RNA and DNA level, respectively, indicating that *SLFN12* is expressed in response to viral load (Fig. 7b, c). To further test whether SLFN12 may be involved in post-transcriptional HIV-1 latency control in vivo, patient's PBMCs were treated with or without LRAs (Romidepsin and Ingenol), stained with anti-Gag-p24 and anti-SLFN12 antibodies plus anti-HIV-1-RNA probes, and analyzed by FISH-Flow assays as previously described<sup>65,66</sup>. The gating strategy is shown in Fig. 7d. SLFN12 expressions in p24 positive(+), HIV-1-RNA+/ p24 negative(-), and both negative populations were characterized (Fig. 7e, f). SLFN12-expressing cells were enriched in the population of HIV-1-RNA+/ p24 - cells, which



is consistent with a role in post-transcriptional HIV-1 latency control.

**Discussion**

The factors and mechanisms that maintain HIV-1 latency and thus hamper antiviral cure strategies are incompletely understood. Here we demonstrate that SLFN12, a member of the conserved family of

Schlafen proteins, is an HIV-1 restriction factor that inhibits HIV-1 translation in a codon-usage dependent manner and participates in virus containment in homeostatically proliferating CD4+ T cells. The mechanism of action of SLFN12 was similar to that of the previously described SLFN11, despite a limited sequence homology between the two Schlafen family members. As the two genes showed differences in their transcription patterns, their antiviral



**Fig. 5 SLFN12-mediated inhibition of HIV-1 translation is codon-usage dependent.** **a** Histogram of codon adaptation indices (CAIs) for the human RefSeq transcript hg38. CAIs of HIV-1 sequences, *GAPDH* and *EGFP* are highlighted for comparison. The mean CAI of human transcripts was 0.77. Gag-opt, codon-optimized gag sequence as in plasmid pGag-opt. **b** Experimental outline. HEK 293T cells were co-transfected with expression plasmids encoding mCherry-fused SLFN11 or SLFN12, or mCherry alone, and an HIV-1 vector expressing Gag-p24 with either wild-type (pGag-wt) or optimized codon usage (pGag-opt). At 48 h post-transfection, transfected cells were lysed and analyzed by Western blot and RT-qPCR. **c, d** Upper panel: Western blot detection of p24 from HEK 293T cells expressing wild-type Gag (Gag-wt, **c**) or codon-optimized Gag (Gag-opt, **d**). Lower panel: Relative HIV-1-gag RNA levels from indicated expression vectors ( $n = 3$  biological replicates; mean  $\pm$  SD). There were no significant differences between the RNA levels amongst the indicated samples (Student's  $t$  test). **e** Heatmap of relative synonymous codon usage of human (*H. sapiens*), HIV-1, HIV-2 and Chikungunya virus (CHIKV) transcripts. Codons Leu-UUA (Leu(TTA) in the graph) and Leu-CUG (Leu(CTG)) are highlighted with arrows. **f** SLFN11 and SLFN12 specifically inhibit Leu-UUA codon-swapped EGFP expression ( $n = 3$  biological replicates; mean  $\pm$  SD). The upper panel shows the outline of the experiment. Wild-type EGFP expression vector (WT) or Leu codon-swapped vectors (Leu-CUG, Leu-CUC, Leu-UUA, Leu-CUU, Leu-UUG, and Leu-CUA) were individually transfected together with mCherry (MOCK), mCherry-fused-SLFN11 or 12 expression vector into HEK 293T cells. After 48 h, relative mean fluorescence intensities (MFI) were measured by flow cytometry. The fold change MFI values are shown; the MFI of mock transfection was set to 1. The asterisks represent statistical significance ( $*p < 0.02$ , by one sample  $t$ -test).

functional redundancy may indicate a way to ensure virus control under different cell growth conditions.

Homeostatic proliferation is a physiological process that restores the peripheral T cell pool after lymphopenia. It requires the cytokines IL-7 and IL-15, and HLA-restricted T cell receptor triggering of low affinity<sup>67</sup>. Importantly, these conditions allow HIV-1-infected T cells to expand without virus production<sup>12,13</sup>. Our previous observations with latently infected primary CD4+ T cells under HSP culture conditions<sup>16</sup>, and that of Mohammadi et al. using another primary CD4+ T cell model of HIV-1 latency<sup>68</sup>, suggested that virus production from provirus-containing cells can be restricted by a post-transcriptional rather than a transcriptional block. Our work here now suggests that SLFN12 is an important component of this post-transcriptional block. It may enable HIV-1-infected cells to remain undetectable to adaptive immune responses and antiviral therapies because the underlying effector mechanisms require viral protein expression for exerting their antiviral function. Consequently, blocking SLFN11 and SLFN12 function and thus, increasing viral protein production would help expose HIV-1 infected cells more effectively to the immune system and antiviral drugs. This should lead to increased HIV-1-infected cell elimination by the immune system and the reduction of the latent reservoir of infected cells in vivo. Studies in this direction are clearly worth pursuing.

Functionally, SLFN gene members have multiple and divergent biological roles in host defense<sup>45–49</sup>, cell differentiation<sup>69,70</sup> and cancer drug sensitivity<sup>58,61,71,72</sup>. SLFNs 5, 11, 13 and 14 have been described as virus restriction factors showing activities against diverse RNA and DNA viruses while SLFN12 until now was considered a candidate antiviral protein based solely on the result of high-throughput screens for interferon-induced antiviral factors<sup>42–44</sup>. Our present work here extends these studies and demonstrates the mechanism by which SLFN12 inhibits HIV-1 and restricts latency reversal in a codon usage-dependent manner. Interestingly, SLFN11 and 12 showed comparable anti-HIV-1 properties that in both cases were abrogated by active site mutations in the proteins' RNase domains. However, the type II tRNA decrease by SLFN12 was less than that by SLFN11 (Supplementary Fig. 5). This observations is in line with recent findings of a specific cleavage of the low abundant Leu-UUA tRNA by SLFN12<sup>60</sup> and the broader cleavage activity of SLFN11<sup>61,63</sup>. In addition, while the C-terminal helicase domain of SLFN11 seems required for its anti-HIV-1 activity<sup>62</sup>, SLFN12 lacks this region and thus exerts its antiviral activity without it. Furthermore, SLFN11 also encodes a nuclear localization signal while SLFN12 does not. Thus, the two SLFN proteins might exert their effect from both the nuclear as well as the cytoplasmic compartment of the cell. Supposing that the antiviral mechanism is mediated by the tRNA cleavage activity as demonstrated for SLFN11<sup>61–63</sup> and

SLFN13<sup>49</sup>, and suggested for SLFN12 here as well (Fig. 6a–f), an effect in the nucleus where the tRNA is generated and in the cytoplasm where the tRNA is used for mRNA-directed translation would be most effective. However, many unknowns with respect to the regulation of the RNase activities of SLFN11 and SLFN12 as well as their possible individual and combined effects on the tRNA pool under different cellular growth conditions remain and require further studies.

Our data from a cohort of HIV-1-infected individuals showed a positive correlation between *SLFN12* expression and HIV-1 viral load (Fig. 7a–c), suggesting a link with the general activation of the immune system. Indeed, *SLFN* family gene expression is considered interferon-inducible<sup>42,43,73,74</sup>. Furthermore, our transcriptome-based identification of *SLFN12* was derived from the screening of homeostatic proliferating primary CD4+ T cells ex vivo (Fig. 1). This mode of proliferation requires the cytokines IL-7 and IL-15 whose expression in vivo is directly linked to reduced CD4+ T cell counts, and high HIV-1 loads<sup>75–77</sup>. Interestingly, *SLFN12* was just one amongst several candidate HIV-1 restriction factors induced under these conditions (Fig. 1c–g), thus suggesting that CD4+ T cells during homeostatic proliferation expand highly protected.

To finally evaluate whether SLFN12 restricts HIV-1 protein expression at a post-transcriptional level ex vivo, we combined FISH-Flow assays to detect intracellular HIV-1 RNA with anti-Gag-p24 and anti-SLFN12 antibody staining and analyzed PBMCs of several infected individuals. A trend towards the enrichment of SLFN12 expression within HIV-1-RNA+/p24– cells was observed in these patients. The same was true when considering the mean fluorescence intensities of SLFN12-expressing cells. This supports our in vitro-experiments with HIV-1-infected cell lines and suggests that SLFN12 also restricts the generation of infectious HIV-1 in people living with HIV (PLWH). However, the frequency of HIV-1 RNA+ and/or p24+ CD4+ T cells within the PBMCs of HIV-1-infected individuals was low (0.01~0.1%), and the current FISH-flow analysis is technically limited in that it cannot discriminate whether infected cells containing complete and competent HIV-1 proviruses from those with defectives forms. Therefore, our observations should be interpreted with caution.

In conclusion, SLFN12 now adds to the growing number of restriction factors that a host utilizes to downregulate HIV-1 production. Importantly, by blocking virus protein production at a translational level, SLFN11 and 12 also help HIV-1 and infected cells to escape from antiviral therapy and avoid immune-mediated destruction, facilitating the virus to reside within its host organism. This makes SLFN11 and 12 interesting therapeutic targets in strategies aiming to eliminate HIV-1 persistence. An experimental examination of this interesting hypothesis clearly deserves further consideration.

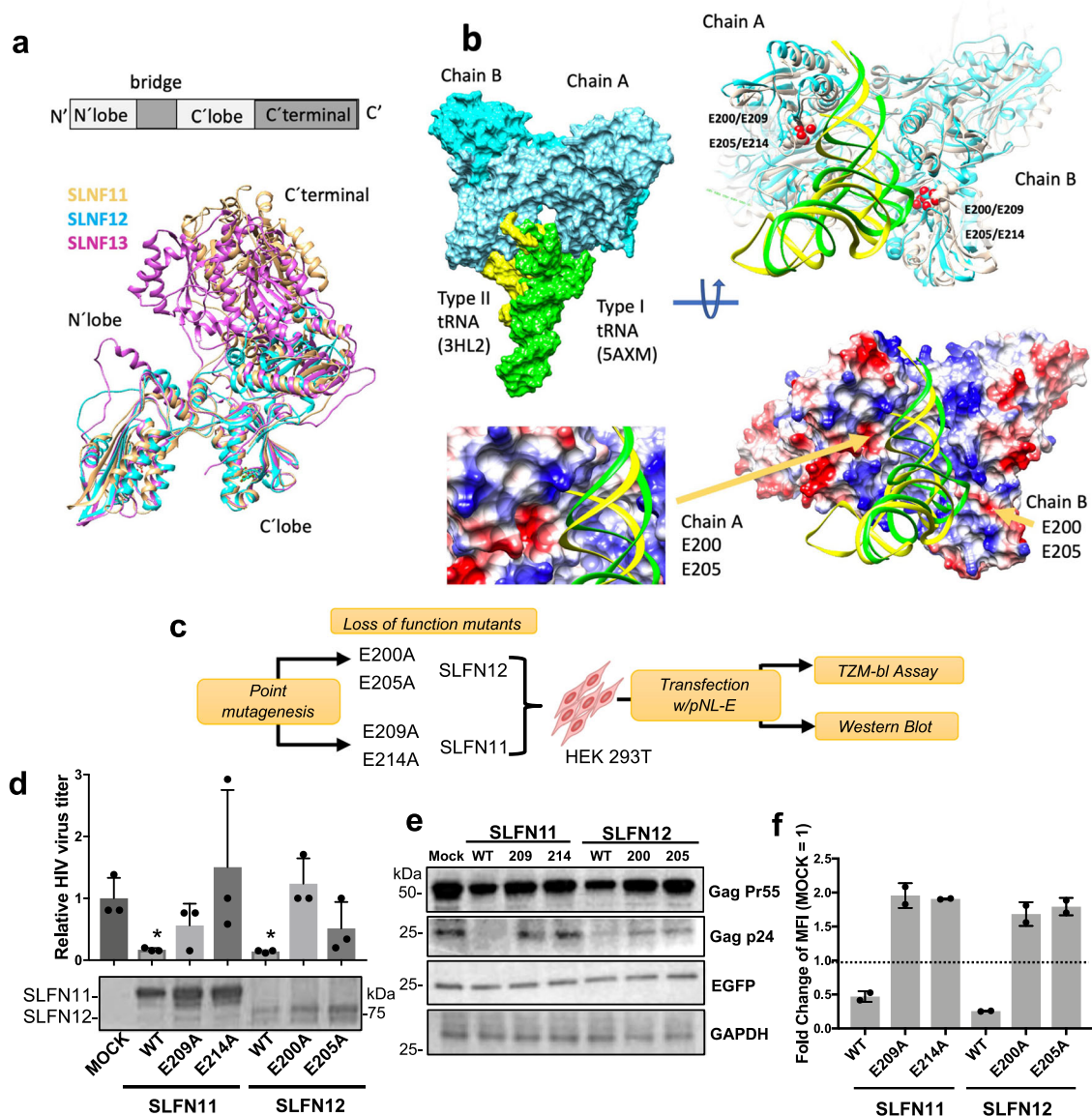


**Fig. 6 SLFN12-mediated HIV-1 suppression depends on a putative tRNase cleavage domain.** **a** Conformational similarity of human SLFN11 (beige), SLFN12 (cyan) and SLFN13 (magenta). Monomer structures retrieved from the cryo-EM structures of SLFN12 (7LRE) and SLFN11 (7ZEL), and from AlphaFold predicted model of SLFN13 (downloaded from Uniprot, code Q68D06) were superimposed and compared in ribbon plates obtained with Chimera<sup>88</sup>. SLFN12 has a short C-terminal domain. **b** Structural models of SLFN12 dimer/trRNA complexes. The cryo-EM structure of SLFN12 dimer (7LRE) docked with the structure of type II tRNA (selenocysteine tRNA, 3HL2) and relaxed, adding the relaxed structure of type I tRNA<sup>Phe</sup> (5AXM) for comparison, are shown as surface representations (chain A of SLFN12 in light blue, chain B of SLFN12 in cyan, type II tRNA in yellow and type I tRNA in green). In the upper right is shown in ribbon plates a comparison of the structures of SLFN11 (7ZEL) and the relaxed model of SLFN12 docked with type I (green) and type II (yellow) tRNAs, highlighting in van der Waals spheres the side-chain atoms of E200 and E205 of SLFN12, and E209 and E214 of SLFN11, of both chains. In the bottom are shown the surface of the relaxed structure of SLFN12, colored by Coulombic potential the positively (red) and negatively (blue) charged areas, plus a ribbon plate of the structures of type I and type II tRNAs, with arrows pointing to the positions of E200 and E205 in both chains and a detailed view of the active site in chain A. The positively charged surface of SLFN12 was responsible of the binding of the tRNA helping to locate the tRNA in a cleft close to the active site formed by glutamates E200 and E205. **c** Experimental outline. mCherry-fused SLFN expression vectors or their respective active site mutants E209A and E214A of SLFN11, and E200A and E205A of SLFN12 were individually co-transfected with HIV-1 pNL-E vector into HEK 293T cells. 48 h post-transfection, cells and supernatants were harvested and processed for further analyses as indicated. The following results are from three independent experiments (**d**, **e**). **d** Mutants of the tRNase cleavage sites of SLFN12 lose their anti-HIV-1 activity (mean  $\pm$  SD). Asterisks indicate significant differences compared to MOCK-transfected cells calculated by Student's *t* test. The lower panel shows expression levels of the SLFN proteins in a Western blot using an anti-mCherry antibody. **e** Western blot showing intracellular HIV-1 Gag Pr55 and p24 levels in SLFN-expressing cells. EGFP and GAPDH were used as controls. **f** The Leu-UUA codon swapped vector was transfected with indicated SLFN mutant expression vectors into HEK 293T cells. After 48 h, relative mean fluorescence intensity (MFI) was measured by flow cytometry. The fold change MFI values are shown; the MFI of mock transfection was set to 1 ( $n = 2$  biological replicates; mean  $\pm$  SD).

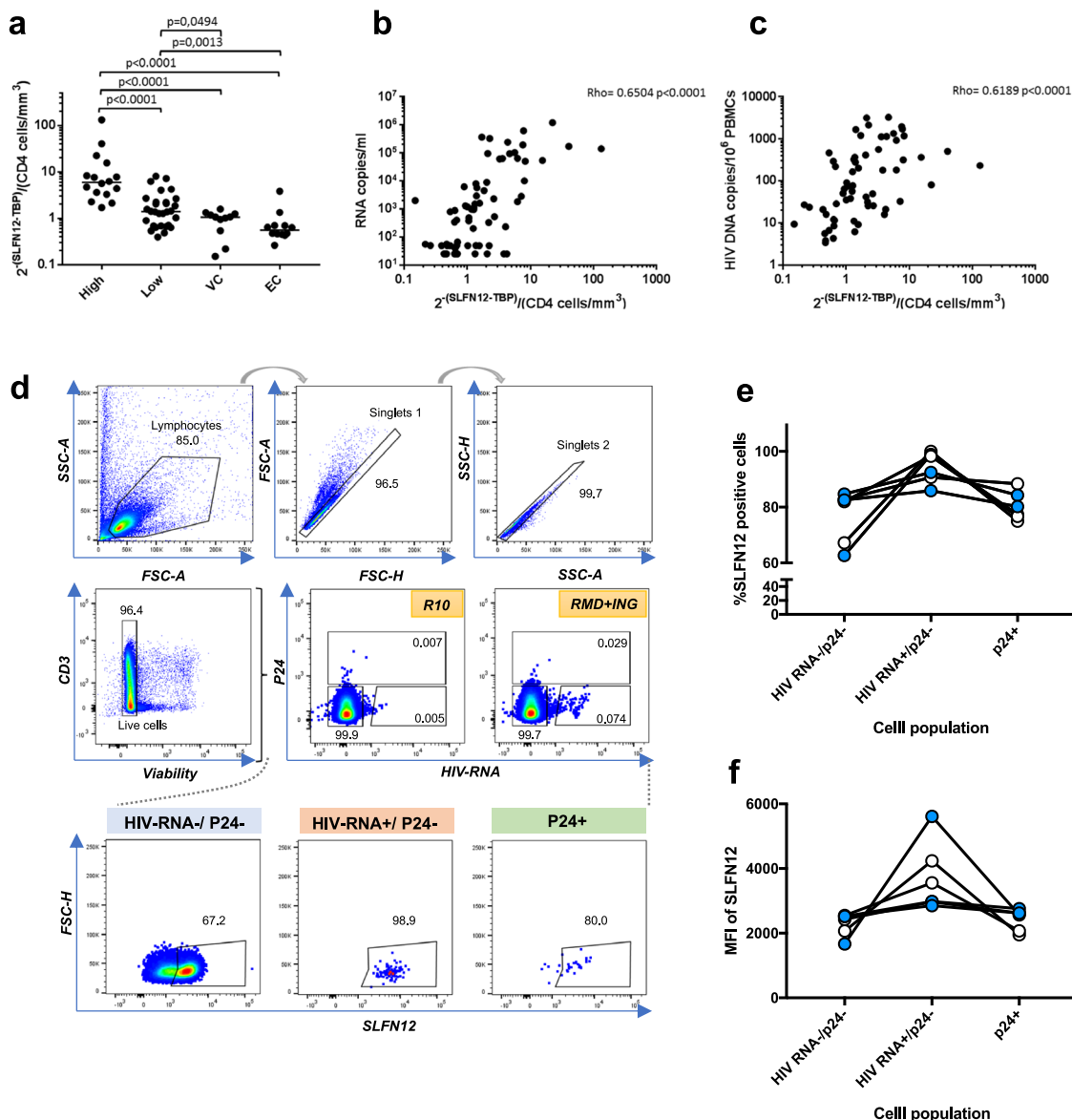


**Fig. 7 Involvement of *SLFN12* gene in HIV-1 post-transcriptional restriction in patients.** **a** Expression level of *SLFN12* in PBMCs from HIV-1-infected individuals without ART. *SLFN12* RNA levels were quantified using PBMCs from HIV-1 high viremic- (High,  $n = 16$ ) and low viremic- (Low,  $n = 30$ ) patients, and viremic- (VC,  $n = 11$ ) and elite-controllers (EC,  $n = 12$ ). *SLFN12* levels were normalized by *TBP* RNA levels and CD4+ T cell counts per  $\mu$ l. Each point represents the values of a single individual. p-values were calculated by Mann-Whitney test. **b** Correlation between *SLFN12* expression levels and viral RNA loads. Each point represents the values of a single individual. The correlation was calculated by Spearman’s rank test. **c** Correlation between *SLFN12* expression levels and HIV-1 provirus loads. Each point represents the values of a single individual. Spearman’s rank test was applied to analyze the correlation. **d-f** *SLFN12* expressing CD4+ T cells are enriched in HIV-1 RNA+/p24- cells. Gating strategy to measure *SLFN12* expression in CD4+ T cells from patients on suppressive ART (**d**). Gating strategy consisted of selecting lymphocytic cells (“Lymphocytes” on the plots) by FSC- and SSC-scatter, followed by a double doublet exclusion (“Singlets1” and “Singlets2”), dead cells exclusion (“Live cells”) and finally an HIV-1-RNA+ and p24+ gate from where *SLFN12*+ cells were identified. The proportion of *SLFN12* expressing cells (**e**) or relative MFI of *SLFN12* (**f**) in p24-/HIV-1 RNA-, p24-/HIV-1 RNA+, or p24+ cells. Blue circles, patient samples treated with Romidepsin plus Ingenol (RMD + ING in **d**) ex vivo ( $n = 3$ ); White circles, untreated patient samples (R10 in **d**,  $n = 3$ ).

**Limitation of the study.** The physiological conditions under which *SLFN11* and/or *SLFN12* restrict HIV-1 expression and suppress latency reversal in vivo are not completely defined. This includes infected cell types e.g. CD4+ T cells and macrophages, location of function e.g. nuclear or cytoplasmic, and the activation of the RNase activity of the SLFNs.

**Methods**

**Ethics statement.** PBMCs from healthy donors and HIV-1 infected patients were obtained with a written consent and by a protocol which was approved by the ethic

committees in the Hospital Universitari Vall d’Hebron (PR(AG)270/2015), and IrsiCaixa (CEIC: EO-12-042 and PI-18-183) in Barcelona, Spain. Experiments with HIV-1-infected cells were conducted at biosafety level 3 (BSL3) facilities at the Universitat Pompeu Fabra, Hospital Universitari Vall d’Hebron and IrsiCaixa.

**Cell lines and PBMCs.** ACH2 cells (NIH AIDS Reagent Program) were cultured in RPMI medium (Gibco) supplemented with 10% heat-inactivated fetal bovine serum (FBS, Sigma Aldrich) and 1% of penicillin/streptomycin mix (P/S, Gibco). HEK 293T cells (ATCC) and TZM-bl cells (NIH AIDS Reagent Program) were maintained in DMEM medium (Gibco) supplemented with 10% heat-inactivated FBS and 1% P/S. All cell lines were incubated at 37 °C in presence of 5% CO<sub>2</sub>. PBMC were isolated by Histopaque-1077 density centrifugation. The separation and culture of



naive CD4+ T cells were conducted according to our previous study<sup>16</sup>. The culture conditions used in this study were as follows: HSP condition – cell cultured with IL-15 and –7 (10 µg/ml, PeprTech); HSP + TCR condition – cells cultured with IL-15 and –7 and activated by anti-CD3 (5 µg/ml, BD Biosciences) and CD28 (1 µg/ml, BD Biosciences) on day 12; TCR condition – cells activated with anti-CD3/CD28 antibodies on day 0 and cultured with IL-2 (2 ng/ml, PeprTech); TCR + TCR condition – cells activated with anti-CD3/CD28 on day 0, cultured with IL-2 and second time activated with anti-CD3/CD28 at day 12.

**RNA-sequencing and bioinformatic analysis.** Total RNA from cultured cells was isolated according to the manufacturer's instructions using Qiagen RNeasy Micro kit (Qiagen) and submitted to the Genomics Unit of Centre for Genomic Regulation (CRG, PRBB, Spain) for sequencing. Quality and concentration of RNA were determined by an Agilent Bioanalyzer. Sequencing libraries were generated by a Ribo-Zero kit (Illumina). cDNA was synthesized and tagged by addition of barcoded Truseq adapters. Libraries were quantified using the KAPA Library Quantification Kit (KapaBiosystems) prior to amplification with Illumina's cBot. Four libraries were pooled and sequenced (single strand, 50nts) on an Illumina HiSeq2000 sequencer to obtain 50–60 million reads per sample. RNA-seq reads were mapped against the Homo sapiens reference genome (GRCh37.p13) with the GEMtools RNA-seq pipeline ([http://gemtools.github.io/docs/rna\\_pipeline.html](http://gemtools.github.io/docs/rna_pipeline.html)). Genes were quantified with the same pipeline using the Gencode version 19 as an annotation. Normalization was performed with the edgeR TMM method<sup>78</sup>. The k-means clustering was performed by iDEP. 94 interface<sup>17</sup> and the heatmap was generated by ggplot2 R package. Gene ontology (GO) enrichment analysis was performed with DAVID (<http://david.ncifcrf.gov/>). Differentially expression analysis was performed with the 'robust' version of the edgeR R package<sup>79</sup>. Genes with FDR < 5% were considered differentially expressed. The list of human gene families was obtained from the HUGO gene nomenclature committee (<https://www.genenames.org/>). The list of HIV-interacting genes and restriction factors were obtained from the NIH HIV interaction database<sup>18–20</sup> and a previous report<sup>28</sup>, respectively.

**RNA isolation and quantitative PCR.** Total RNA was extracted from cells and treated with DNase I according to the manufacturer's instructions using Qiagen RNeasy Mini Kit (Qiagen). 100–1000 ng RNA was reverse-transcribed into cDNA in a total volume of 20 µl using SuperScript IV Reverse Transcriptase (ThermoFisher). 2 µl of cDNA was used for quantitative PCR (qPCR) in a 10 µl reaction using SYBR master mix (ThermoFisher). Each reaction was performed in triplicates in 384-well plates in a QuantStudio 12K flex (ThermoFisher). Relative RNA levels were calculated after normalization to 18S rRNA unless specified otherwise. Primers used this study are described in Supplementary Data 7.

For *SLFN12* expression quantification in HIV-1 participants, total RNA samples from available PBMC dry-pellets were obtained using Qiagen RNeasy Mini Kit (Qiagen) following manufacturer's recommendations. cDNA was obtained using SuperScript IV Reverse Transcriptase (ThermoFisher) and TaqMan gene expression assay (Applied Biosystems) was used for detection of *SLFN12* (Hs00430118\_m1) and *TBP* (Hs99999910\_m1). Gene amplification was performed on an Applied Biosystems 7500 Fast Real-Time PCR System thermocycler, and the relative expression was calculated as  $2^{-\Delta CT}$  (where CT is the median threshold cycle from 3 replicates).

Quantification of integrated HIV-1-proviral DNA was performed from PBMC by droplet digital PCR (ddPCR) as described<sup>80</sup>. Briefly, two different primer/probe sets annealing to the 5' long terminal repeat (LTR) and *gag* regions, respectively, were used to circumvent sequence mismatch in the patient proviruses, and the *RPP30* housekeeping gene was quantified in parallel to normalize sample input. Raw ddPCR data were analyzed using the QX100™ droplet reader and QuantaSoft v1.6 software (Bio-Rad).

**Plasmids.** *SLFN11/12* sequences were acquired from the plasmids clone MGS: 59997 (*SLFN11*) and clone MGS: 45076 (*SLFN12*) provided by Dharmaco and cloned into mCherry expression vector, pmCherry-N' (Clontech) between NheI and HindIII restriction sites. The plasmids generated were named pmCherry-SLFN11 and pmCherry-SLFN12, respectively. pNL-E, the HIV-1 proviral clone pNL4-381-derived *EGFP*-expressing plasmid, was generated previously<sup>50</sup>. The plasmid expressing HIV-1 wild-type *gag* sequence in pEF-BOS\_bsr backbone was produced previously (pGag-wt)<sup>82</sup>. To generate HIV-1 codon-optimized *gag* expressing plasmid (pGag-opt), the codon-optimized *gag* sequence was obtained from the plasmid p96ZM651gag-opt (Drs. Y. Li, F. Gao, and B.H. Hahn through the National Institutes of Health (NIH) AIDS Reagent Program, Reference# 8675) and ligated between BamHI and NotI sites of pEF-BOS\_bsr. Retrovirus vectors carrying shRNA sequences were constructed by inserting annealed oligonucleotides into a pSIN-siU6 vector (Takara) between BamHI and ClaI sites. As a negative control pSIN-siU6 vector expressing shRNA scramble sequences was used<sup>83</sup>. The constructs expressing mutant SLFNs (*SLFN11* E209A, *SLFN11* E214A, *SLFN12* E200A and *SLFN12* E205A) were generated using Q5 Site-Directed Mutagenesis Kit (NEB). The mutagenesis was performed according to the substitution protocol using primers designed with the NEBaseChanger (NEB). Codon-swapped *EGFP*

expression vectors were produced previously<sup>61</sup>. The primers and shRNA sequences utilized here are listed in Supplementary Data 7.

**Transfection and transduction.** Transduction and transfection were done according to our previous study<sup>84</sup>. To prepare recombinant retroviruses carrying the shRNAs, HEK 293T cells were seeded in a 6-well plate at a density of  $6 \times 10^5$  cells/well and co-transfected with pSIN-siU6 – shSLFN11/ shSLFN12/ shSc (2 µg) along with plasmids pGP (1 µg, Takara) and pPE amphi (1 µg, Takara) using 12 µl of Lipofectamine 2000 (ThermoFisher) per well. At 48 h after transfection, the supernatant was harvested and added on to ACH2 cells (1 ml of supernatant/ $10^5$  cells). Transduction was performed by spinoculation ( $1200 \times g$ , 25 °C, 2 h). Pelleted cells were resuspended in 500 µl of RPMI with 10% FBS and placed into 24-well plates. Selection of transduced cells was done by adding G418 (1 mg/ml, InvivoGen) into the cell at 48 h after transduction.

For the expression studies in HEK 293T cells, the cells were seeded in 24-well plate at a density of  $2 \times 10^5$ , and after 24 h co-transfected with construct pmCherry-SLFN11/ pmCherry-SLFN12 along with vector HIV-1-pNL-E, pGag-wt, pGag-opt, or codon-swapped EGFP using Lipofectamine 2000 (2.5 µl/well). At 3–4 h post transfection, fresh medium was replaced, and the cells were kept at 37 °C with 5% CO<sub>2</sub> for 24 or 48 h.

**SAHA treatment of ACH cells.** ACH2 cells with blocked expression of SLFN11 and SLFN12 (as described above) were seeded in a 24-well plate and treated with DMSO (0.01%, Sigma-Aldrich) or SAHA (Vorinostat, Sigma-Aldrich) at 0.5 µM. The cells were lysed for RNA or protein isolation at 48 h after treatment. Supernatants were harvested at 72 h after treatment to test for virus titer by TZM-bl assay.

**TZM-bl assay.** Virus titers in supernatants from transfected HEK 293T cells and HIV-1-reactivated ACH2 cells were determined by the TZM-bl assay as described previously<sup>85</sup>. Briefly, 11 serial dilutions of supernatants were prepared and added into fresh TZM-bl cells ( $10^4$  cells/well) in 96-well flat-bottom culture plates (Greiner Bio-One). After 72 h incubation at 37 °C, 5% CO<sub>2</sub> the luciferase activity was measured on Centro LB 960 Microplate Luminometer (Berthold Technologies) using Britelite Plus™ (PerkinElmer) according to the manufacturer's protocol. Based on the luciferase levels, the TCID<sub>50</sub> was calculated.

**Western blot and antibodies.** The cells were lysed with 1× passive lysis buffer (Promega), snap-frozen in liquid nitrogen and kept at –80 °C overnight. The next day, cell debris was removed by centrifugation at 15,000 RPM for 5 min and supernatants were mixed with 2× Laemmli buffer, heated at 97 °C for 5 min, transferred to the nitrocellulose membrane and immunoblot using specific antibodies was performed. Detection was done using secondary antibodies conjugated with horseradish peroxidase (HRP). Protein bands were developed on Medical X-Ray Blue Films (AGFA) using Pierce™ ECL Plus Western Blotting Substrate or SuperSignal WestFemto Maximum Sensitivity Substrate (ThermoFisher) and quantified in Image-J software. The antibodies used in this study are listed in Supplementary Data 8.

**Flow cytometry.** CD4+ T cells after HSP or TCR culture were incubated with LIVE/DEAD® Fixable Aqua (ThermoFisher) and human Fc blocker (BD Bioscience). Then the cells were washed and stained with anti-CD4, CD8, CD27, and CD45RO- antibodies (Supplementary Data 8) on ice for 20 min. Transfected HEK 293T cells were suspended with PBS containing 1% FBS and 1 µg/mL 4',6-diamidino-2-phenylindole (DAPI) before data acquisition. Fluorescence was measured on a BD LSRFortessa (Becton, Dickinson) and analyzed with FlowJo v10 (Becton, Dickinson).

**Polysome profiling.** HEK 293T were co-transfected with pmCherry/ pmCherry-SLFN11/ pmCherry-SLFN12 (12 µg) and HIV-1-pNL-E (12 µg) using Lipofectamine 2000 (48 µl) in a T-150 culture dish (ThermoFisher). In order to freeze elongation ribosomes, 48 h after transfection cells were treated with 10 ml of DMEM containing cycloheximide (CHX, 100 µg/ml) during 2 min at 37 °C and washed with 10 ml of PBS containing CHX (100 µg/ml) using a vacuum system. Cells were lysed with 700 µl of lysis buffer (10 mM Tris-HCl (pH = 7.4), 10 mM MgCl<sub>2</sub>, 100 mM NaCl, 1% Triton X100, 2 mM DTT, 100 µg/ml CHX), scraped and immediately frozen in liquid nitrogen and stored at –80 °C. Cell lysates were thawed at 25 °C and centrifuged at  $12,000 \times g$ , 5 min, 4 °C and the supernatants were transferred to new tubes. After quantification, aliquots of 8 U<sub>A260</sub> were made and stored at –80 °C. Linear gradients of 10–50% sucrose were prepared in polysome buffer (20 mM Tris-HCl (pH = 7.4), 10 mM MgCl<sub>2</sub>, 100 mM NH<sub>4</sub>Cl). The Gradient Master (Biocomp) was used to prepare the gradients in polyallomer tubes (Beckman Coulter). One aliquot of 8 U<sub>A260</sub> was loaded on each gradient and centrifuged in Beckman SW41 rotor at 35 000 RPM, 3 h, 4 °C. Gradients were fractionated with fraction collector Model 2128 (BioRad). These fractions were used for phenol:chloroform RNA extraction and analyzed by RT-qPCR.

**Structural comparison.** The dimer structures of human SLFN11 and SLFN12 were downloaded from PDB<sup>86</sup> (codes 7ZEL and 7LRE, respectively). A model of the monomeric structure of SLFN13 was downloaded from Uniprot (model predicted by AlphaFold<sup>87</sup>, AF-Q68D06-F1). The model of the dimer structure of SLFN13 was constructed by superimposition on the structure of SLFN11 with the program Matchmaker using Chimera software (version 1.13.1)<sup>88</sup>. The model of the complex of SLFN12 with yeast tRNA<sup>Phe</sup> Type I was obtained by docking the structure of the dimer of SLFN12 with the tRNA structure (code 5AXM) according to Metzner et al.<sup>63</sup> using SLFN11 as template. The model of the complex of SLFN12 with human selenocystein tRNA Type II was obtained by docking it with the tRNA structure (code 3HL2) according to Yang et al.<sup>49</sup> using SLFN13 as template. The structures of the complexes were relaxed and optimized with Rosetta<sup>89</sup> and ribbon plates and surfaces, colored by Coulombic potential, were calculated and plotted with Chimera (version 1.13.1)<sup>88</sup>.

**Calculating and visualizing gene-wise CAI and RSCU.** For all hg38 RefSeq genes, we used the seqinr (v.3.3-6) and ggplot2 (3.1.0) R-packages and codon weights obtained from CAIcal ([http://genomes.urv.es/CAIcal/CU\\_human\\_nature](http://genomes.urv.es/CAIcal/CU_human_nature)). We used Codon Usage Table database (<https://hive.biochemistry.gwu.edu/cuts/about>) for calculation of RSCU<sup>55</sup>.

**FISH-flow.** PBMC from ART-treated HIV-1-infected patients were obtained from the HIV Unit of the Hospital Universitari Vall d'Hebron (Barcelona, Spain) and CD4+ T cells were isolated by negative selection using magnetic beads (MagniSort Human CD4+ T Cell Enrichment; eBioscience). CD4+ T cells were then stimulated during 22 h with latency-reversing agents (LRAs; 40 nM Romidepsin (Selleckchem) plus 100 nM Ingenol-3-angelate (Sigma-Aldrich)), or the negative control (media alone, R10; RPMI medium supplemented with 10% FBS). Prior to viral reactivation, cells were pre-incubated with the pan-caspase inhibitor Q-VD-Oph for 2 h. In order to block new rounds of viral infections during viral reactivation, cells were treated with LRAs in the presence of Raltegravir (1  $\mu$ M), Darunavir (1  $\mu$ M) and Nevirapine (1  $\mu$ M). Cells were then subjected to the RNA FISH/flow protocol for the detection of HIV-1 transcripts and the viral protein Gag-p24 following the manufacturer's instructions (Human PrimeFlow RNA Assay; eBioscience) with some modifications, as previously described<sup>66</sup>. In these experiments, to identify CD4+ T cells expressing SLFN12, HIV-1 RNA and the viral protein p24, the following antibodies were used: for cell surface staining, CD3 (PE-Cy7, BD Biosciences); and for SLFN12 detection, after fixation and permeabilization steps, cells were stained with primary rabbit anti-SLFN12 (Abcam) followed by incubation with a secondary donkey anti-rabbit IgG (AF488, Invitrogen) for 30 min at room temperature. The expression of HIV-1 RNA transcripts was analyzed with HIV-1 gag-pol-specific AF647-labeled probes, and the expression of the Gag-p24 viral protein was detected with a PE-anti-p24 antibody (clone KC57 RD1; Beckman Coulter). Cell viability was determined using an aqua viability dye for flow cytometry (LIVE/DEAD® Fixable Aqua Dead Cell Stain kit, Invitrogen).

**Statistics and reproducibility.** Student's *t* test (two-sided), one-sample *t*-test, ratio paired *t*-test, Mann-Whitney test, one-way ANOVA, or Spearman's rank test (specified in each figure legend) were applied for the study. *p*-values <0.05 were considered statistically significant. The number of replicates were described in each figure legend.

**Patient information.** Classification of HIV-1 infected individuals was according to their HIV-1 RNA copies/mL (pVL) plus their history of ART in the past year. The criteria were as follows: (i) HIV-1 high viremic patients (HIV-High); >50,000pVL, (ii) HIV-1 low viremic patients (HIV-Low); <10,000pVL without ART, (iii) elite controllers (EC); <50pVL without ART, (iv) Viremic controllers (VC); <2000pVL without ART. The pVLs and CD4 counts of each patient group are summarized in Supplementary Table 1.

**Cytoplasmic and nuclear RNA isolation.** HEK293T cells were transfected with pmCherry/ pmCherry-SLFN11/ pmCherry-SLFN12 along with HIV-pNL-E. Twenty-four hours after transfection, the cells were lysed with lysis buffer (10 mM Tris-HCl (pH=7.5), 10 mM NaCl, 1.5 mM MgCl<sub>2</sub>, 10 mM Vanadyl complex (NEB), 1% NP-40 (Sigma-Aldrich) and kept on ice for 5 min. After centrifugation at 3000 RPM for 5 min at 4 °C, the supernatant (cytoplasmic fraction) was transferred to a new tube and the nuclear pellet was resuspended in a lysis buffer without Vanadyl complex and MgCl<sub>2</sub>. To extract RNA from each fraction, an equal volume of Roti-Aqua-Phenol (Carl Roth, Germany) was added and centrifuged at 16,000  $\times$  g for 5 min at room temperature. The aqueous phase was transferred into a new tube and subjected to chloroform extraction and ethanol precipitation. The ethanol precipitation was done by adding 0.3 volumes of 3 M Sodium Acetate, 3 volumes of 100% EtOH (Merck) and 1  $\mu$ l of glycogen (Roche). After 15 min incubation at -80 °C, samples were centrifuged for 15 min at 16,000  $\times$  g at 4 °C. The supernatant was discarded, and the pellet was resuspended in 1 ml of 70% EtOH and centrifuged for 5 min at 16,000  $\times$  g at 4 °C. The RNA pellet was dissolved in Diethyl Pyrocarbonate (DEPC)-treated water. DNA was removed by TURBO DNA-free kit (Ambion). Expression levels of HIV-gag RNA and HIV total RNA were analyzed by RT-qPCR.

**RNA gel electrophoresis.** Transfected HEK 293T cells were collected and subjected to total RNA extraction through phenol-chloroform extraction as described above. 2  $\mu$ g of RNA were resolved in a 10% TBE-Urea polyacrylamide gel. Bands of tRNA and 5.8S rRNA were visualized by ethidium bromide staining and quantified by Image J.

**Reporting summary.** Further information on research design is available in the Nature Portfolio Reporting Summary linked to this article.

## Data availability

The RNA-seq data from this study are available from the NCBI Expression Omnibus GEO; GSE221332. Gating strategy of flow cytometry performed in Figs. 1b, 5f and 6f are shown in Supplementary Figs. 6 and 7. Uncropped version of Western blot images are available from Supplementary Figs. 8 to 11. The numerical source data are provided in Supplementary Data 9–15. All other data are available from the corresponding authors on reasonable request.

Received: 9 January 2023; Accepted: 13 April 2023;

Published online: 10 May 2023

## References

- Siliciano, J. D. & Siliciano, R. F. In vivo dynamics of the latent reservoir for HIV-1: new insights and implications for cure. *Annu. Rev. Pathol.* **17**, 271–294 (2022).
- Fromentin, R. & Chomont, N. HIV persistence in subsets of CD4+ T cells: 50 shades of reservoirs. *Semin. Immunol.* **51**, 101438 (2021).
- Liu, R., Simonetti, F. R. & Ho, Y. C. The forces driving clonal expansion of the HIV-1 latent reservoir. *Viol. J.* **17**, 4 (2020).
- Douek, D. C. et al. HIV preferentially infects HIV-specific CD4+ T cells. *Nature* **417**, 95–98 (2002).
- Simonetti, F. R. et al. Clonally expanded CD4+ T cells can produce infectious HIV-1 in vivo. *Proc. Natl. Acad. Sci. USA* **113**, 1883–1888 (2016).
- Grossman, Z. et al. 'Rinse and replace': boosting T cell turnover to reduce HIV-1 reservoirs. *Trends Immunol.* **41**, 466–480 (2020).
- Cesana, D. et al. HIV-1-mediated insertional activation of STAT5B and BACH2 trigger viral reservoir in T regulatory cells. *Nat. Commun.* **8**, 498 (2017).
- Ikeda, T., Shibata, J., Yoshimura, K., Koito, A. & Matsushita, S. Recurrent HIV-1 integration at the BACH2 locus in resting CD4+ T cell populations during effective highly active antiretroviral therapy. *J. Infect. Dis.* **195**, 716–725 (2007).
- Maldarelli, F. et al. HIV latency. Specific HIV integration sites are linked to clonal expansion and persistence of infected cells. *Science* **345**, 179–183 (2014).
- Wagner, T. A. et al. HIV latency. Proliferation of cells with HIV integrated into cancer genes contributes to persistent infection. *Science* **345**, 570–573 (2014).
- Chen, H. C., Martinez, J. P., Zorita, E., Meyerhans, A. & Filion, G. J. Position effects influence HIV latency reversal. *Nat. Struct. Mol. Biol.* **24**, 47–54 (2017).
- Bosque, A., Famiglietti, M., Weyrich, A. S., Goulston, C. & Planelles, V. Homeostatic proliferation fails to efficiently reactivate HIV-1 latently infected central memory CD4+ T cells. *PLoS Pathog* **7**, e1002288 (2011).
- Chomont, N. et al. HIV reservoir size and persistence are driven by T cell survival and homeostatic proliferation. *Nat. Med.* **15**, 893–900 (2009).
- Drake, A. et al. Interleukins 7 and 15 maintain human T cell proliferative capacity through STAT5 signaling. *PLoS One* **11**, e0166280 (2016).
- Rochman, Y., Spolski, R. & Leonard, W. J. New insights into the regulation of T cells by gamma(c) family cytokines. *Nat. Rev. Immunol.* **9**, 480–490 (2009).
- Tsunetsugu-Yokota, Y. et al. Homeostatically maintained resting naive CD4(+) T cells resist latent HIV reactivation. *Front. Microbiol.* **7**, 1944 (2016).
- Ge, S. X., Son, E. W. & Yao, R. iDEP: an integrated web application for differential expression and pathway analysis of RNA-Seq data. *BMC Bioinformatics* **19**, 534 (2018).
- Fu, W. et al. Human immunodeficiency virus type 1, human protein interaction database at NCBI. *Nucleic Acids Res.* **37**, D417–D422 (2009).
- Pinney, J. W. et al. HIV-host interactions: a map of viral perturbation of the host system. *AIDS* **23**, 549–554 (2009).
- Ptak, R. G. et al. Cataloguing the HIV type 1 human protein interaction network. *AIDS Res. Hum. Retroviruses* **24**, 1497–1502 (2008).
- Chen, H. et al. A critical role for CD63 in HIV replication and infection of macrophages and cell lines. *Virology* **379**, 191–196 (2008).
- Fu, E. et al. Tetraspanin CD63 is a regulator of HIV-1 replication. *Int. J. Clin. Exp. Pathol.* **8**, 1184–1198 (2015).
- Li, G., Dziuba, N., Friedrich, B., Murray, J. L. & Ferguson, M. R. A post-entry role for CD63 in early HIV-1 replication. *Virology* **412**, 315–324 (2011).



24. Tippett, E., Cameron, P. U., Marsh, M. & Crowe, S. M. Characterization of tetraspanins CD9, CD53, CD63, and CD81 in monocytes and macrophages in HIV-1 infection. *J. Leukoc. Biol.* **93**, 913–920 (2013).
25. Li, M. et al. TIM-family proteins inhibit HIV-1 release. *Proc. Natl. Acad. Sci. USA* **111**, E3699–E3707 (2014).
26. Duggal, N. K. & Emerman, M. Evolutionary conflicts between viruses and restriction factors shape immunity. *Nat. Rev. Immunol.* **12**, 687–695 (2012).
27. Ito, J., Gifford, R. J. & Sato, K. Retroviruses drive the rapid evolution of mammalian APOBEC3 genes. *Proc. Natl. Acad. Sci. USA* **117**, 610–618 (2020).
28. Abdel-Mohsen, M. et al. Expression profile of host restriction factors in HIV-1 elite controllers. *Retrovirology* **10**, 106 (2013).
29. Adelson, M. E., Martinand-Mari, C., Iacono, K. T., Muto, N. F. & Suhadolnik, R. J. Inhibition of human immunodeficiency virus (HIV-1) replication in SupT1 cells transduced with an HIV-1 LTR-driven PKR cDNA construct. *Eur. J. Biochem.* **264**, 806–815 (1999).
30. Muto, N. F., Martinand-Mari, C., Adelson, M. E. & Suhadolnik, R. J. Inhibition of replication of reactivated human immunodeficiency virus type 1 (HIV-1) in latently infected U1 cells transduced with an HIV-1 long terminal repeat-driven PKR cDNA construct. *J. Virol.* **73**, 9021–9028 (1999).
31. Wu, Y., Zhang, Z., Li, Y. & Li, Y. The regulation of integrated stress response signaling pathway on viral infection and viral antagonism. *Front. Microbiol.* **12**, 814635 (2021).
32. Harding, H. P. et al. An integrated stress response regulates amino acid metabolism and resistance to oxidative stress. *Mol. Cell* **11**, 619–633 (2003).
33. Nakabayashi, K. et al. Genomic imprinting of PPP1R9A encoding neurabin 1 in skeletal muscle and extra-embryonic tissues. *J. Med. Genet.* **41**, 601–608 (2004).
34. Tsujimoto, Y. & Shimizu, S. Bcl-2 family: life-or-death switch. *FEBS Lett.* **466**, 6–10 (2000).
35. Raghunath, M. et al. A novel kinase, AATYK induces and promotes neuronal differentiation in a human neuroblastoma (SH-SY5Y) cell line. *Brain Res. Mol. Brain Res.* **77**, 151–162 (2000).
36. Guy, G. R., Jackson, R. A., Yusoff, P. & Chow, S. Y. Sprouty proteins: modified modulators, matchmakers or missing links? *J. Endocrinol.* **203**, 191–202 (2009).
37. Chakrabarti, A. et al. RNase L activates the NLRP3 inflammasome during viral infections. *Cell Host Microbe* **17**, 466–477 (2015).
38. Player, M. R., Maitra, R. K., Silverman, R. H. & Torrence, P. F. Targeting RNase L to human immunodeficiency virus RNA with 2-5A-antisense. *Antivir. Chem. Chemother.* **9**, 225–231 (1998).
39. Han, Y. et al. Structure of human RNase L reveals the basis for regulated RNA decay in the IFN response. *Science* **343**, 1244–1248 (2014).
40. Ghosh, H. S., Spencer, J. V., Ng, B., McBurney, M. W. & Robbins, P. D. Sirt1 interacts with transducin-like enhancer of split-1 to inhibit nuclear factor kappaB-mediated transcription. *Biochem. J.* **408**, 105–111 (2007).
41. Liu, L. et al. Nucling interacts with nuclear factor-kappaB, regulating its cellular distribution. *FEBS J.* **276**, 1459–1470 (2009).
42. Kane, M. et al. Identification of interferon-stimulated genes with antiretroviral activity. *Cell Host Microbe* **20**, 392–405 (2016).
43. Liu, S. Y., Sanchez, D. J., Aliyari, R., Lu, S. & Cheng, G. H. Systematic identification of type I and type II interferon-induced antiviral factors. *Proc. Natl. Acad. Sci. USA* **109**, 4239–4244 (2012).
44. Kim, E. T. & Weitzman, M. D. Schlafens can put viruses to sleep. *Viruses* **14**, <https://doi.org/10.3390/v14020442> (2022).
45. Li, M. et al. Codon-usage-based inhibition of HIV protein synthesis by human schlafen 11. *Nature* **491**, 125–128 (2012).
46. Kim, E. T. et al. Comparative proteomics identifies Schlafens 5 (SLFN5) as a herpes simplex virus restriction factor that suppresses viral transcription. *Nat. Microbiol.* **6**, 234–245 (2021).
47. Seong, R. K. et al. Schlafens 14 (SLFN14) is a novel antiviral factor involved in the control of viral replication. *Immunobiology* **222**, 979–988 (2017).
48. Valdez, F. et al. Schlafens 11 restricts flavivirus replication. *J. Virol.* **93**, <https://doi.org/10.1128/JVI.00104-19> (2019).
49. Yang, J. Y. et al. Structure of Schlafens13 reveals a new class of tRNA/rRNA-targeting RNase engaged in translational control. *Nat. Commun.* **9**, 1165 (2018).
50. Yamamoto, T. et al. Selective transmission of R5 HIV-1 over X4 HIV-1 at the dendritic cell-T cell infectious synapse is determined by the T cell activation state. *PLoS Pathog.* **5**, e1000279 (2009).
51. Varenne, S., Buc, J., Llobelis, R. & Lazdunski, C. Translation is a non-uniform process. Effect of tRNA availability on the rate of elongation of nascent polypeptide chains. *J. Mol. Biol.* **180**, 549–576 (1984).
52. Yu, C. H. et al. Codon usage influences the local rate of translation elongation to regulate co-translational protein folding. *Mol. Cell* **59**, 744–754 (2015).
53. Sharp, P. M. & Li, W. H. The codon Adaptation Index—a measure of directional synonymous codon usage bias, and its potential applications. *Nucleic Acids Res.* **15**, 1281–1295 (1987).
54. van Weringh, A. et al. HIV-1 modulates the tRNA pool to improve translation efficiency. *Mol. Biol. Evol.* **28**, 1827–1834 (2011).
55. Athey, J. et al. A new and updated resource for codon usage tables. *BMC Bioinformatics* **18**, 391 (2017).
56. Berkhout, B. & van Hemert, F. J. The unusual nucleotide content of the HIV RNA genome results in a biased amino acid composition of HIV proteins. *Nucleic Acids Res.* **22**, 1705–1711 (1994).
57. Vartanian, J. P., Meyerhans, A., Asjo, B. & Wain-Hobson, S. Selection, recombination, and G→A hypermutation of human immunodeficiency virus type 1 genomes. *J. Virol.* **65**, 1779–1788 (1991).
58. Chen, J. et al. Structure of PDE3A-SLFN12 complex and structure-based design for a potent apoptosis inducer of tumor cells. *Nat. Commun.* **12**, 6204 (2021).
59. Garvie, C. W. et al. Structure of PDE3A-SLFN12 complex reveals requirements for activation of SLFN12 RNase. *Nat. Commun.* **12**, 4375 (2021).
60. Lee, S. et al. Velcrin-induced selective cleavage of tRNA(Leu)(TAA) by SLFN12 causes cancer cell death. *Nat. Chem. Biol.* **3**, 301–310 (2022).
61. Li, M. et al. DNA damage-induced cell death relies on SLFN11-dependent cleavage of distinct type II tRNAs. *Nat. Struct. Mol. Biol.* **25**, 1047–1058 (2018).
62. Malone, D., Lardelli, R. M., Li, M. & David, M. Dephosphorylation activates the interferon-stimulated Schlafens family member 11 in the DNA damage response. *J. Biol. Chem.* **294**, 14674–14685 (2019).
63. Metzner, F. J. et al. Mechanistic understanding of human SLFN11. *Nat. Commun.* **13**, 5464 (2022).
64. Brennan, T. & Sundaralingam, M. Structure of transfer RNA molecules containing the long variable loop. *Nucleic Acids Res.* **3**, 3235–3250 (1976).
65. Grau-Exposito, J. et al. Latency reversal agents affect differently the latent reservoir present in distinct CD4+ T subpopulations. *PLoS Pathog.* **15**, e1007991 (2019).
66. Grau-Exposito, J. et al. A novel single-cell FISH-flow assay identifies effector memory CD4(+) T cells as a major niche for HIV-1 transcription in HIV-infected patients. *mBio* **8**, <https://doi.org/10.1128/mBio.00876-17> (2017).
67. Shevryev, D., Tereshchenko, V., Manova, O. & Kozlov, V. Homeostatic proliferation as a physiological process and a risk factor for autoimmune pathology. *AIMS Allergy Immunol.* **5**, 18–32 (2021).
68. Mohammadi, P. et al. Dynamics of HIV latency and reactivation in a primary CD4+ T cell model. *PLoS Pathog.* **10**, e1004156 (2014).
69. Patel, V. B., Yu, Y., Das, J. K., Patel, B. B. & Majumdar, A. P. Schlafens-3: a novel regulator of intestinal differentiation. *Biochem. Biophys. Res. Commun.* **388**, 752–756 (2009).
70. Schwarz, D. A., Katayama, C. D. & Hedrick, S. M. Schlafens, a new family of growth regulatory genes that affect thymocyte development. *Immunity* **9**, 657–668 (1998).
71. Lewis, T. A. et al. Optimization of PDE3A modulators for SLFN12-dependent cancer cell killing. *ACS Med. Chem. Lett.* **10**, 1537–1542 (2019).
72. Takashima, T. et al. Schlafens 11 predicts response to platinum-based chemotherapy in gastric cancers. *Br. J. Cancer* **125**, 65–77 (2021).
73. Mavrommatis, E., Fish, E. N. & Plataniias, L. C. The Schlafens family of proteins and their regulation by interferons. *J. Interferon Cytokine Res.* **33**, 206–210 (2013).
74. Puck, A. et al. Expression and regulation of Schlafens (SLFN) family members in primary human monocytes, monocyte-derived dendritic cells and T cells. *Results Immunol.* **5**, 23–32 (2015).
75. Llano, A. et al. Interleukin-7 in plasma correlates with CD4 T-cell depletion and may be associated with emergence of syncytium-inducing variants in human immunodeficiency virus type 1-positive individuals. *J. Virol.* **75**, 10319–10325 (2001).
76. Napolitano, L. A. et al. Increased production of IL-7 accompanies HIV-1-mediated T-cell depletion: implications for T-cell homeostasis. *Nat. Med.* **7**, 73–79 (2001).
77. Swaminathan, S. et al. Interleukin-15 (IL-15) strongly correlates with increasing HIV-1 viremia and markers of inflammation. *PLoS One* **11**, e0167091 (2016).
78. Robinson, M. D. & Oshlack, A. A scaling normalization method for differential expression analysis of RNA-seq data. *Genome Biol.* **11**, R25 (2010).
79. Zhou, X., Lindsay, H. & Robinson, M. D. Robustly detecting differential expression in RNA sequencing data using observation weights. *Nucleic Acids Res.* **42**, e91 (2014).
80. Oriol-Tordera, B. et al. Methylation regulation of Antiviral host factors, Interferon Stimulated Genes (ISGs) and T-cell responses associated with natural HIV control. *PLoS Pathog.* **16**, e1008678 (2020).
81. Adachi, A. et al. Production of acquired immunodeficiency syndrome-associated retrovirus in human and nonhuman cells transfected with an infectious molecular clone. *J. Virol.* **59**, 284–291 (1986).
82. Yoshizawa, I. et al. Enhancement of mucosal immune response against HIV-1 Gag by DNA immunization. *Vaccine* **19**, 2995–3003 (2001).

83. Yamagishi, M. et al. Retroviral delivery of promoter-targeted shRNA induces long-term silencing of HIV-1 transcription. *Microbes Infect.* **11**, 500–508 (2009).
84. Kobayashi-Ishihara, M. et al. HIV-1-encoded antisense RNA suppresses viral replication for a prolonged period. *Retrovirology* **9**, 38 (2012).
85. Brai, A. et al. Human DDX3 protein is a valuable target to develop broad spectrum antiviral agents. *Proc. Natl. Acad. Sci. USA* **113**, 5388–5393 (2016).
86. Burley, S. K. et al. RCSB Protein Data Bank: celebrating 50 years of the PDB with new tools for understanding and visualizing biological macromolecules in 3D. *Protein Sci* **31**, 187–208 (2022).
87. Varadi, M. et al. AlphaFold Protein Structure Database: massively expanding the structural coverage of protein-sequence space with high-accuracy models. *Nucleic Acids Res.* **50**, D439–D444 (2022).
88. Huang, C. C., Meng, E. C., Morris, J. H., Pettersen, E. F. & Ferrin, T. E. Enhancing UCSF Chimera through web services. *Nucleic Acids Res.* **42**, W478–W484 (2014).
89. Conway, P., Tyka, M. D., DiMaio, F., Konerding, D. E. & Baker, D. Relaxation of backbone bond geometry improves protein energy landscape modeling. *Protein Sci.* **23**, 47–55 (2014).

## Acknowledgements

We thank Drs Yingying Li, Feng Gao and Beatrice H. Hahn for providing codon-optimized HIV-1 Gag expression vector, Drs James Hoxie and Susan Zolla-Pazner for supplying anti-Nef and -p24 antibodies, respectively through the NIH AIDS reagent program. We also thank Dr Song Gao for providing SLFN13-tRNA structure information, and Dr Maria-Eugenia Gas Lopez and Dr Ester Gea-Mallorqui for advise. This work was supported by following grants: M.K.I., JSPS Oversea Research Fellowship and Takeda Science Foundation; A.E.C., PT17/0009/0019 (ISCIII/MINECO and FEDER); M.J.B., RTI2018-101082-B-I00 and PID2021-123321OB-I00 [MINECO/FEDER]), and the Miguel Servet program by ISCIII (CP17/00179 and CPII22/00005); C.B., M.R.R., C.D.C., European Union's Horizon 2020 research and innovation program under grant agreement 681137-EAVI2020 and NIH grant P01-AI131568; J.D., the Spanish Ministry of Science and Innovation (PID2019106959RB-I00/AEI/10.13039/501100011033); A.M., the Spanish Ministry of Science and Innovation (PID2019-106323RB-I00 AEI//10.13039/501100011033) and the institutional "María de Maeztu" Programme for Units of Excellence in R&D (CEX2018-000792-M).

## Author contributions

M.K.I., J.P.M., Y.T.Y., J.A., J.D. and A.M. designed the research study. M.K.I., K.F.S., J.P.M., Y.T.Y., F.E.A., K.G., M.G., J.G.E., C.D.C., and S.R. performed the experiments. J.J., M.L., M.D., and M.Y. provided essential tools. A.E.C., R.B., B.O., M.R.R., and M.J.B.

analyzed the data. M.K.I., K.F.S., and A.M. wrote the manuscript. J.A., J.P.M., C.B., and J.D. critically discussed the manuscript. All authors have read and approved the final manuscript.

## Competing interests

S.R. is an employee of Novartis, Switzerland. J.P.M. is an editor of Nature Communications. C.B. is a founder, CSO, and shareholder of AELIX THERAPEUTICS. The rest of the authors declare no competing interests.

## Additional information

**Supplementary information** The online version contains supplementary material available at <https://doi.org/10.1038/s42003-023-04841-y>.

**Correspondence** and requests for materials should be addressed to Mie Kobayashi-Ishihara, Juana Díez or Andreas Meyerhans.

**Peer review information** *Communications Biology* thanks Heidi Greulich and the other anonymous reviewer(s) for their contribution to the peer review of this work. Primary Handling Editors: Zhijuan Qiu and Karli Montague-Cardoso. Peer reviewer reports are available.

**Reprints and permission information** is available at <http://www.nature.com/reprints>

**Publisher's note** Springer Nature remains neutral with regard to jurisdictional claims in published maps and institutional affiliations.



**Open Access** This article is licensed under a Creative Commons Attribution 4.0 International License, which permits use, sharing, adaptation, distribution and reproduction in any medium or format, as long as you give appropriate credit to the original author(s) and the source, provide a link to the Creative Commons license, and indicate if changes were made. The images or other third party material in this article are included in the article's Creative Commons license, unless indicated otherwise in a credit line to the material. If material is not included in the article's Creative Commons license and your intended use is not permitted by statutory regulation or exceeds the permitted use, you will need to obtain permission directly from the copyright holder. To view a copy of this license, visit <http://creativecommons.org/licenses/by/4.0/>.

© The Author(s) 2023